Reactivity Controlled Compression Ignition for clean and efficient ship propulsion

Accepted Manuscript

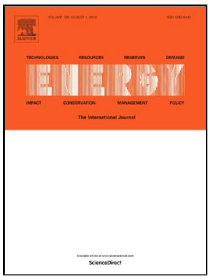

Reactivity Controlled Compression Ignition for Clean and Efficient Ship Propulsion

Maciej Mikulski, Sudarshan Ramesh, Cemil Bekdemir

PII:	S0360-5442(19)31223-X
DOI:	10.1016/j.energy.2019.06.091
Reference:	EGY 15574
To appear in:	*Energy*
Received Date:	21 December 2018
Accepted Date:	12 June 2019

Please cite this article as: Maciej Mikulski, Sudarshan Ramesh, Cemil Bekdemir, Reactivity Controlled Compression Ignition for Clean and Efficient Ship Propulsion, *Energy* (2019), doi: 10.1016/j.energy.2019.06.091

REACTIVITY CONTROLLED COMPRESSION IGNITION FOR CLEAN AND EFFICIENT SHIP PROPULSION

ABSTRACT

Reactivity Controlled Compression Ignition (RCCI) is commonly mentioned as a potential efficient and clean combustion concept. This study makes the first evaluation of natural gas-diesel RCCI combustion for mid-speed marine engines.

A state-of-the-art dual-fuel engine with 350 mm bore diameter is the basis for numerical simulations. GT-Power is used to create a one-dimensional air-path model. RCCI is simulated using TNO's multi-zone combustion model incorporating detailed chemical kinetics. The simulations aim to optimize engine efficiency, with peak in-cylinder pressure and emissions as constraints.

The study shows best-point Indicated Efficiency of 47.8% is achievable (@75% load) using RCCI mode on stock engine hardware, while meeting IMO Tier III's NO_x limit. This performance is similar to the best contemporary marine gas engines, but RCCI also provides additional methane and CO emission reductions. Thus, RCCI combustion can meet Europe's new rigorous Stage V limits, offering significant improvements in a marine engine's GHG footprint.

Crucially, the study indicates an engine using hardware optimized for RCCI could deliver outstanding indicated efficiencies of 52%, with emissions of below 1g/kWh for all legislative species. This combination of high efficiency and ultra-low emissions would make RCCI combustion an attractive proposition for future marine propulsion and gen-set applications.

KEYWORDS: RCCI, mid-speed engine, marine, natural gas, simulation; energy optimization

1. INTRODUCTION

The 2020 global sulphur regulation will have a major impact on marine propulsion system development. Over 70,000 ships [1, 2] must switch from Heavy Fuel Oil (HFO) to Marine Gas Oil (MGO) fuel with a low sulphur content (0.1/0.5 %) or install a scrubber. The first option increases fuel costs: the second involves major investment and eats into cargo space. And both options will also need the addition of urea-based Selective Catalytic Reduction (SCR) system in order to meet International Maritime Organization (IMO) Tier III NO_x limits. This entails extra investment and adds the running costs of the SCR system (urea and maintenance). Additionally, mid-speed marine engines still must prove compliance with upcoming restrictive emission legislation for European inland waterways (Stage V) and for Chinese domestic emission control areas (China II) [3, 4].

Impending emissions legislation creates a strong drive for alternative, cleaner power options in maritime and inland shipping. Liquefied Natural Gas (LNG) is a short and medium-term alternative for conventional Compression Ignition (CI) engines. LNG availability is increasing, it is cheaper than MGO and cuts CO2 (low carbon-content fuel), soot and NO_x emissions.

Contemporary gas propulsion systems use either a stratified charge (lean-burn) spark-ignited (SI) concept or a dual-fuel (DF) approach. Lean-burn, spark ignited (LBSI) mid-speed marine engines are currently offered by manufacturers such as Wärtsilä [5] and Rolls Royce [6]. They use additional, low-pressure gas injection directly to the pre-chamber to make the mixture locally rich and easily ignitable with a spark plug [7, 8]. Wärtsilä reported brake thermal efficiencies (BTE) above 48% and peak load of 22 bar Brake Mean Effective Pressure (BMEP) for their 34SG engine [5]. The engines meet the International Maritime Organization (IMO) Tier III limits.

Cho et al. offer a good overview of current SI gas engines research [9]. More recently, Shah et al. [10] investigated the lean-burn SI concept for possible efficiency improvement. The authors used a single-cylinder research engine modified from a Wärtsilä 6-cylinder, 200 mm-bore mid-speed unit. The geometrical compression ratio (CR)

of 13 was used, while the effective CR was 12 due to the applied Miller timing. The study focused on optimizing the pre-chamber to main chamber volume ratio and corresponding equivalence ratios. The investigation aimed at determining the best efficiency/ NO_x trade-off at one particular mid-load operating point. The optimum was found at the main chamber λ of 1.8 and relative pre-chamber volume of 2.4%. The authors reported that 51% Indicated Gross Efficiency (η_{Igross}) is achievable with these settings while meeting Tier III's NO_x limit. Other ways of improving the efficiency of mono-fuel LB concept focus on sophisticated ignition systems to widen the lean operation window [11].

Wei and Geng provide a comprehensive review of NG/diesel dual-fuel combustion, emissions and performance [12]. Minimizing NO_x and soot emissions and achieving the greatest greenhouse gas reduction benefits involves maximizing the NG-diesel blend ratio and combining it with lean operation for knock resistance and high thermal efficiency. The so-called lean burn dual fuel engine (LBDF) engine operates with the air-fuel ratio around 2:1 and reducing the diesel pilot injection to around 1% of total fuel energy [13]. Combustion, despite compression ignited, is dominated by flame propagation. This makes it similar to lean-burn SI engines, with similar benefits and requirements for air-path configuration and control. The concept is therefore often referred to as liquid spark ignition. The two concepts also share similar drawbacks: difficult controllability and large cycle-to-cycle variations, limiting optimization potential [13]. The optimum high-load operational window is very narrow for both systems and limited by knock and misfire. The additional advantages of a micro-pilot engine compared to SI are fewer hardware changes (no pre-chamber with Direct Injection (DI) needed) and less frequent maintenance intervals because injectors last longer than spark plugs. Capability to run 100% diesel if LNG is unavailable is another plus for an LBDF engine, but often involves installing two separate injectors – one for main diesel injection, another for micro pilot [13]. LBDF engines are currently offered by MAN Energy Solutions [14], Wärtsilä [15] and some smaller manufacturers, as a solution to meet marine IMO Tier III emission limits for mid-speed, large-bore engines [13]. Claimed efficiency levels are comparable to equivalent diesels.

A few published studies focus on marine DF engine optimization [16-19]. Importantly, Sixtel et al. [18] coupled an in-house combustion model with GT-Power to investigate LBDF combustion on methanol, taking NG operation as the baseline. More recently, Stoumpos et. al. [19] used a similar approach (with Wibe model) to investigate the emission reduction potential of the Wärtsilä 9L50DF platform using different engine measures. The study showed that only a minor (6%) improvement potential in NO_x emissions is attainable within the LBDF concept. The air-path constraints and methane slip tradeoff were identified as main limiting factors.

High-pressure Direct Injection (HPDI) of NG is an alternative DF strategy. In this mode, the diesel pilot is the ignition source and low-reactivity fuel is injected directly into the diesel burn region. Combustion is therefore primarily diffusion-controlled, as in diesel mode, imposing similar requirements for air-path control as for diesel reference [20]. The emission characteristics (PM, NO_x) are slightly different due to different fuel properties. For NG, the adiabatic flame temperature is lower than with diesel, reducing NO_x. However, NO_x and PM reduction potential is far less than with the premixed concepts mentioned earlier [21]. On the other hand, HPDI's late-cycle injection and non-premixed combustion give it an inherent advantage in terms of HC emissions (including CH_4 for NG concepts) [22]. Due to its combustion similarities with a diesel engine, the concept is often referred to as gas-diesel combustion (GD).

The difficulty with using NG as fuel in the HPDI/GD mode lies in compressing gaseous fuel to pressure levels allowing fast injection around Top Dead Center (TDC). Gas-feed pressure in a range of 250-350 bars (depending on engine load) is necessary to allow operation similar to diesel. That entails installing an additional high-pressure gas compressor or a special LNG pump unit. This level of gas compression demands significant compressor power, resulting in a brake efficiency penalty for the engine. Only a fraction of that compression power is needed for an LNG liquid pump yet the available systems are so far unable to reach injection pressures above 300 bar [22]. However, Westport and Bosch are currently independently developing systems capable of reaching 500 bar injection pressure for automotive applications [23, 24]. Both Wärtsilä and MAN made tests with GD engines [25, 26]. In both cases, the engines required around 5% diesel energy share to initiate combustion. Only a slight decrease in engine efficiency was observed compared with the baseline diesel operation. A NO_x emission reduction of around 50% was reported, meeting IMO Tier II level. Importantly, the concept tolerates fuel quality and no engine derating is required for a wide range of NG fuel qualities.

A handful of alternative combustion technologies have emerged recently. Reactivity Controlled Compression Ignition (RCCI) has shown significant advantages over other low-temperature combustion concepts like HCCI or PCCI (respectively, homogenous and premixed charge compression ignition). RCCI uses two fuels, pre-blended in the cylinder to create a reactivity gradient. A small amount of diesel serves as a high-reactivity fuel, injected very early during the compression stroke. This gives good controllability, allowing load-flexible operation, while maintaining high thermal efficiency with ultra-low NO_x and soot [27].

Many research works have been published on RCCI with different fuels. This study's review, covering the use of NG as the low-reactivity fuel in larger RCCI engines (bore size > 120 mm), takes in 18 titles published until the end of 2018. A major contribution comes from TNO [28-31]. Most of the published works are fundamental level studies focusing on particular phenomena and sensitivities, not directly revealing the current status of this technology. Most authors report best results for mid-load (9-13 bar BMEP) engine operation, proving either diesel-like efficiencies with ultra-low (below Euro VI) engine-out NO_x [32, 33] or 2-4 percentage points better efficiencies with a relaxed NO_x limit [34]. The average blend rate (BR) used for optimized conditions varied between 70% and 98 % depending on engine load and hardware. High load is limited by excessive pressure rise rates and P_{max} [35], while efficient low-load operation has low combustion efficiency from insufficient in-cylinder mixing [31].

Researching RCCI for marine engines, Garcia Valladoid et al. [36] tested a range of injection timings, covering both LBDF and RCCI regimes. The experiments were performed on a single-cylinder research engine based on the Wärtsilä 20 DF platform with the same injection aperture. The geometrical compression ratio was 13:1 and two load points were explored: mid-load operation with Indicated Mean Effective Pressure (IMEP) of 10 bar and a high-load point (19 bar IMEP). For both cases, the global equivalence ratio was maintained at 0.5 without using external Exhaust Gas Recirculation (EGR). Both points were initially optimized with energy-based BR of 88% and 95% respectively. The engine incorporated Wartsila's variable valve actuation technology, so late Intake Valve Closing (IVC) reduced the effective compression ratio at high load. Despite the focus being mixture ignitability and cycle-to-cycle variations in different fuel distribution regimes, the research showed retarding diesel injection timing is crucial for ultra-low NO_x levels in DF operation. It found optimized injection timings for a typical RCCI regime were 42-50 Crank Angle (CA) bTDC, where recorded NO_x emissions were below Tier III limits.

Table 1 summarizes the review of the most relevant NG combustion concepts for marine mid-speed engines. Note that trends presented for RCCI are extrapolated from heavy-duty road transport studies since little research on RCCI operation in large-bore engines is available, except Garcia Valladolid's [36].

Table 1: Typical trends in efficiency and emissions for different combustion concepts relative to a state-of-the-art diesel engine Colors indicate performance change within a given category with respect to the best in class solution. Abbreviations: SI - spark ignition, CI - compression ignition, MF - mono-fuel, DF - dual-fuel, BTE - Brake Thermal Efficiency, LB - Lean Burn, TRL – technology readiness level.

	Combustion principle	BR	BTE	CO_2	CH_4	NO_x	Fuel flex	TRL	Technological highlights
SI LB MF, pre-chamber	Premixed, flame propagation	100	=↓	↓ 25-30%	↑↑	↓ 85-90%	No	Proven technology	Major complex modification with gas fueling to each pre-chamber
CI LB DF, micro-pilot	Premixed, flame propagation	90-99%	=↓	↓ 20-30%	↑↑	↓ 80-90%	limited	Proven technology	Separate diesel injectors required for micro pilot and diesel mode
CI DF HPDI, gas-diesel	Non-premixed, spray flame	90-95%	=	↓20-26%	=↑	↓ 30-50%	Yes	Prototype technology	High gas pressure (>300 bar) required (LNG pump or booster compressor)
CI DF RCCI	Part-premixed, reaction kinetics	80-98%	=↑	↓ 20-35%	↑	↓ 80-95%	Yes	Research stage	High load limited by peak pressure and pressure rise rate

Table 1 shows that RCCI could offer better thermal efficiency than diesel but with ultra-low NO_x. CH_4 can still be a challenge, though studies on heavy-duty truck engines showed that meeting Stage V for gas engines is feasible without aftertreatment. Low methane slip and potentially better efficiency contribute to a significantly lower GHG

footprint for RCCI than the best diesel and gas engines. Furthermore, with typically smaller blend ratios than LBDF engines, variations in fuel quality can be handled better and full diesel redundancy can be secured without the need for a dedicated injection system.

Despite these advantages, except initial studies, RCCI on large-bore engines has not been openly demonstrated. It might bring both additional specific benefits and specific difficulties. This work explores the feasibility of applying RCCI combustion on typical, mid-speed, marine engines. The basis for the numerical simulation is a dual-fuel engine. RCCI is simulated with the use of a detailed chemical kinetics model. The primary objective of the simulations is to optimize engine efficiency, with NO_x emissions and peak in-cylinder pressure as engine design constraints.

2. METHODS

Publicly available geometrical data of an MAN 6L35/44DF engine [14, 37, 38] is used to build a GT-Power representation. This state-of-the-art, Tier III engine is designed to accommodate the lean-burn dual-fuel combustion principle using LNG and different types of liquid fuels. The set-up entails diesel fuel injected directly through a separate pilot injector. Natural gas is admitted individually to each cylinder via a gas valve from a low-pressure system (5 bar). Basic technical parameters are provided in Table 2 (Engine A).

The air-path model is further tuned to the in-cylinder pressure data, courtesy of MAN Energy Solutions. The reference indication data came from a single-cylinder research version of the engine, operated on the test bench. With exactly the same cylinder geometry, the proper intake conditions on a test rig are assured using an external compressor and simulated exhaust backpressure to represent real engine operating conditions. The results of the GT-Power model calibration are presented in subsection 2.1. To this end, the model is used to set up boundary conditions for running RCCI on a large-bore engine platform, from the air-path perspective.

RCCI combustion was not explored experimentally on the given platform. The combustion model used to simulate RCCI combustion was originally built and validated on a different engine platform, by TNO. This is a heavy-duty truck engine adopted for RCCI operation with diesel and natural gas. Reference data is provided in Table 2 (Engine B).

Table 2: Technical data of the engines used to identify and validate the models. PFI - Port Fuel Injection.

	Engine A	Engine B
Engine type	Large-bore, mid-speed, 4 stroke 6-cyl in line	Heavy-duty truck size, 4 stroke, 6-cyl in line
Combustion mode	LBDF diesel-NG	RCCI diesel-NG
Rated power /speed	530 kW/cyl at 720 rpm	50 kW/cyl at 1500 rpm
Compression ratio	12:1 (geometrical) *	14:1 (geometrical)
Air path	Variable geometry turbocharger	2 x turbocharger, intake throttle, VVA
EGR path	No	High-pressure, cooling, valve, variable bypass
Injection system	PFI gas, DI common rail diesel	PFI gas, DI common rail diesel
*estimated based on cylinder geometry data provided in [37]		

The combustion model referred to as XCCI is a multi-zone, chemical kinetics-based code meant explicitly to simulate low temperature combustion modes like RCCI. For the purpose of the present study, the model was scaled-up to represent Engine A. Since the model is physics-based and does not make assumptions about engine size and speed that would disqualify its use for marine engines, it is considered adequate for the present work without re-calibration. Note that the flexibility of XCCI on the choice of an engine platform has already been shown in control applications by Indrajuana et. al. [39]. Relevant details of XCCI modelling are presented in subsection 2.2.

The XCCI model for a large-bore engine (engine A) is further used to explore RCCI combustion at representative load points. The investigation aims to find the optimal efficiency point while meeting the set durability and emission limits. This is further discussed in subsection 2.3. (Scope and workflow of RCCI simulations).

2.1 The GT-Power Model

GT-Power software by Gamma Technologies is used to simulate the performance of the engine. This is an industry-standard, one-dimensional, physics-based engine simulation toolchain, widely used for supporting engine (air-path) design process. The air-path model for the considered 6L35/44DF marine engine is built upon the standard, 6-cylinder, direct-injection diesel engine layout provided in GT-Power. Major changes incorporated into the base layout include:

i. cylinder geometry and valve lift profiles of engine A,
ii. pipe diameter and bends at various locations (manifolds, intake & exhaust runners, compressor outlet to intake manifold and from ambient to compressor inlet, exhaust manifold to turbine inlet and from turbine inlet to ambient),
iii. modifying the turbo and compressor maps,
iv. inclusion of an NG injector in each cylinder's intake port.

Geometrical data for building the model comes from the MAN L35/44DF Project Guide [37]. The turbocharger chosen for the 6-cylinder engine is the TCR20-42 model by MAN. For modeling the compressor and the turbine, a standard turbocharger model is scaled up using the characteristic maps provided in the specification sheet of the TCR20-42 [38]. Numerous studies indicate that more favorable conditions for RCCI can be achieved using high EGR rates [28, 31, 34]. This is mainly related to (i) reducing mixture reactivity to avoid premature combustion and (ii) possibility to elevate the thermal state of the in-cylinder charge at IVC (T_{IVC}) [34], which is an important factor influencing combustion efficiency. For these reasons, a high-pressure EGR loop is added to the standard layout of the 6L35/44DF engine.

Figure 1 shows the layout of the developed air-path model, along with the signals used for both simulation input and validation. The multi-cylinder GT-Power model is further tuned to experimental data available from a single-cylinder engine. This is done for the high-load operating point, which is particularly challenging for the air-path. Table 3 shows the basic data of the selected operating point, relevant for the calibration process.

Table 3: Operating point data with signals relevant to the calibration process. SOI = Start of Injection, VTG = Variable Geometry Turbocharger.

100% load – 20 bar BMEP					
Engine Speed	BR	SOI diesel	VTG pos	BPV pos	PCYL
RPM	%	CA	%	deg	bar
720	base	Base	57	90	f(CA)

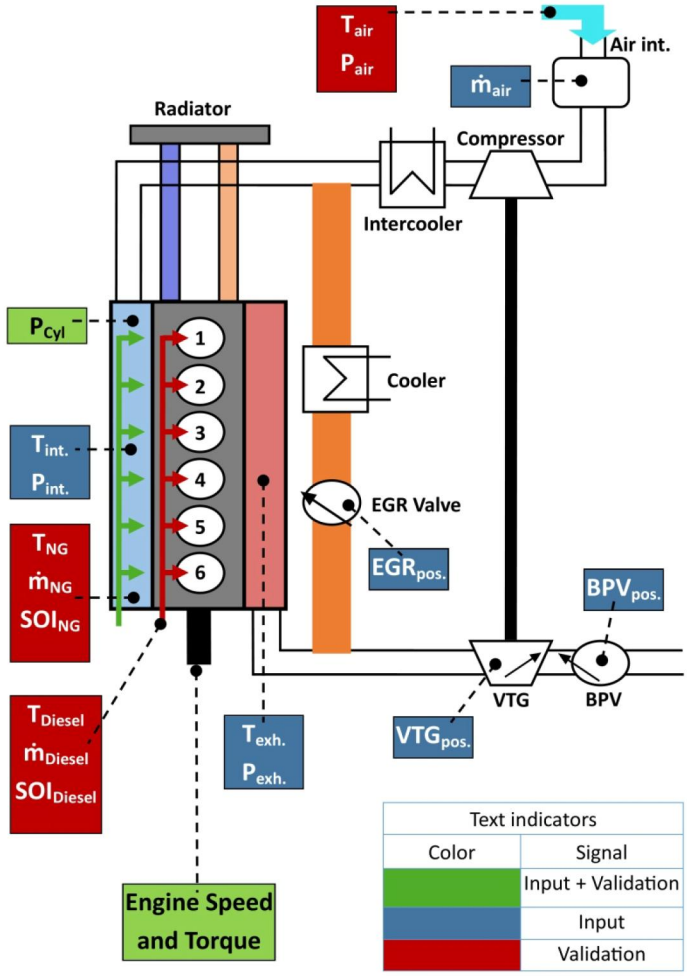

***Fig**. 1: High-level schematic of the GT-power model, along with the signals used as model input and for validation. The additional EGR loop is shown in orange.*

During calibration, the measured average pressure trace from 200 cycles, fuel consumption (both diesel and NG) and SOI of diesel are used as input to the GT-Power model. Variable Turbine Geometry (VTG) position is then adjusted to match the simulation results to the reference experimental data. The desired VTG position is obtained when the simulated pressure trace, fresh air mass flow rate and gross IMEP ($IMEP_{gross}$) match with the measurement results within the cycle-to-cycle accuracy. Figures 2 and 3 give a high-level overview of the validation results in terms of the mentioned parameters. Due to confidentiality restrictions, results are shown as relative quantities with respect to the adopted peak pressure limit (Fig. 2) and the experimental value of the given parameter (Fig. 3).

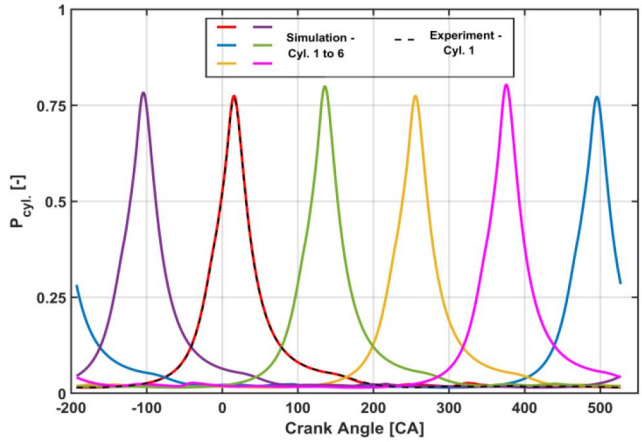

Fig. 2: The pressure trace in simulated in GT-Power for all 6 cylinders vs measured pressure trace from a single-cylinder setup.

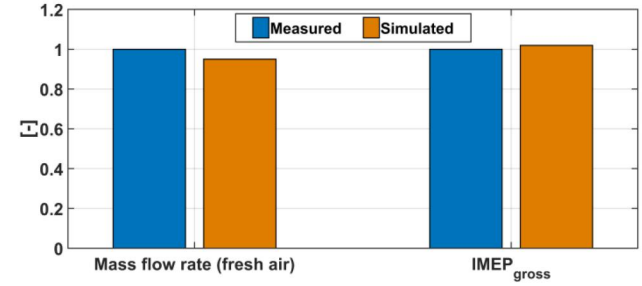

Fig. 3: Measured vs Simulated fresh air mass flow rate and $IMEP_{gross}$ averaged over 200 cycles. The results are shown as relative quantities with respect to the experimental value of the given parameter.

Figures 2 and 3 show the developed GT-Power model predicts fresh air mass flow rate, cylinder pressure and thereby the $IMEP_{gross}$ accurately. The validation results give confidence to use this model as a base for RCCI simulations. The simulations aim to compare the performance of RCCI combustion mode with the baseline LBDF mode, on the same engine hardware, including the limitations and losses associated with the air-path.

2.2 The XCCI combustion model

This section briefly describes the RCCI combustion model used in this research. The multi-zonal RCCI combustion model, developed at TNO and called XCCI, has been previously introduced in [41, 29, 30]. XCCI has also been instrumental in several of TNO's concept studies and applied in model-based control development research [31, 39]. For consistency, only the main features of this combustion model are presented in this section. The governing equations are derived in [41] and, for informative purposes, provided in the appendix A.

The multi-zone model includes complex chemical kinetics computations with flexibility on number of zones, fuels and reaction pathways. The current implementation of the model employs 13 cylindrical zones, with fine discretization near the cylinder walls, to better reflect reactivity and thermal stratification associated with RCCI (Fig. 4). All zones at each time instance have individual temperature and composition while sharing the same pressure. Interaction between zones occurs in the form of mass and heat transfer, governed by a diffusion-driven mixing model. Turbulence enhances mixing and is captured in the model by a coefficient (Turbulent mixing coefficient - Ct) multiplying on the gradient-based transfer. For the goal of the present study, the mixing coefficient is determined for each operating point, based on an empirical correlation with intake pressure and engine speed [42].

The system exchanges heat with the environment across the cylinder head, piston crown (permissible for all the zones) and cylinder liner (the outermost zone only). The process is assumed to be convection-dominated (gas to wall) with the heat transfer coefficient calculated from the formula by Chang et al. [43], designed to calculate heat

exchange in low-temperature combustion engines. Initialization parameters such as the wall surface temperatures of the piston, cylinder head, and liner are individually drawn from engine load, speed and coolant conditions. These phenomena are illustrated in Fig. 4, along with the schematic view of the zonal configuration.

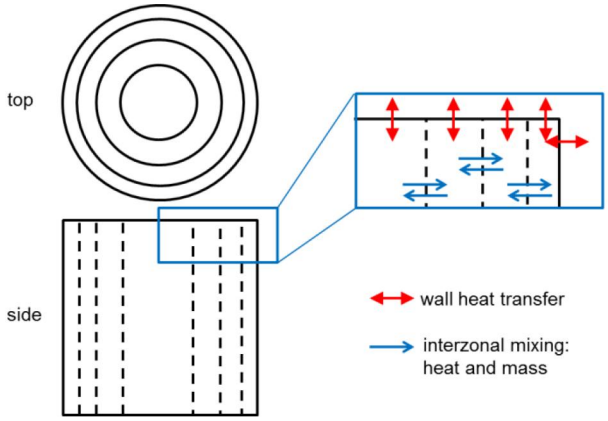

Fig. 4: Graphical representation of the multi-zone RCCI combustion model with cylindrical zonal configuration.

Gaseous fuel is assumed to be homogeneously mixed with air at IVC. During injection, the liquid fuel is introduced to individual zones based on the predefined distribution pattern. This reflects the reactivity stratification, characteristic for early-injection RCCI. Note that the injection model includes heat loss due to fuel evaporation. Combustion is assumed to be fully controlled by reaction kinetics. Reaction progress and the energy equation in each zone are solved using an open-source chemical kinetic solver - Cantera [44], implemented directly to the MATLAB code of XCCI. This study uses combined n-heptane (as diesel surrogate) and NG reaction mechanism, comprised of 65 species and 354 reactions. Specifically, n-heptane is modelled based on the reaction scheme of Peters et al. [45] and the C1-C3 part of the chain is taken from the GRI 3.0 mechanism [46]. The GRI 3.0 scheme also supplies the necessary reaction mechanism for NO_x formation.

RCCI combustion is known to be sensitive to IVC conditions. For instance, natural changes in EGR composition (especially unburned hydrocarbons and partially reformed intermediate species) from cycle to cycle can influence combustion substantially [30]. In order to reflect these sensitivities to intake charge conditions, a detailed valve flow model is coupled with the XCCI code. The simulations are run in a multi-cycle fashion until convergence in resulting pressure trace is reached. Figure 5 shows the full simulation scheme, including relevant inputs and main outputs of the XCCI model.

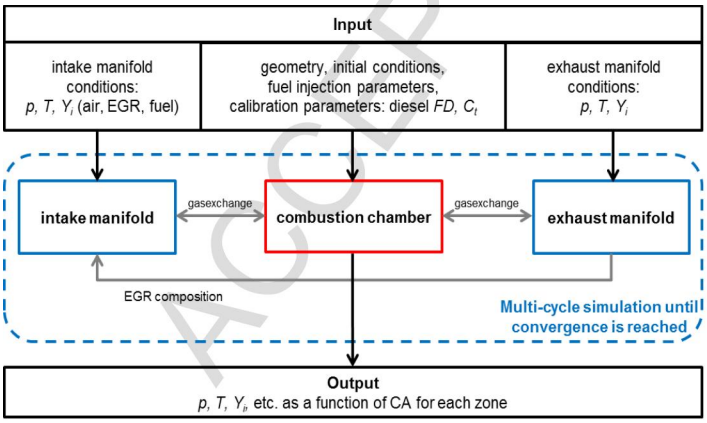

Fig. 5: Schematic view of the multi-zone model simulations.

The model was calibrated and extensively validated on TNO's engine platform (Engine B). Detailed information on methods and results of this work can be found in earlier studies [29, 30, and 31]. XCCI has proven to

be capable of capturing the in-cylinder pressure trace within cycle-to-cycle variations, for a wide range of operating points, showing desired sensitivity on changes in SOI, BR, intake conditions and EGR. This translates to very good accuracy in terms of combustion efficiency and emissions indicators, which are the focuses of the present study. Figure 6 shows high-level results of validation of the model for a representative RCCI load sweep (reproduced from [30]).

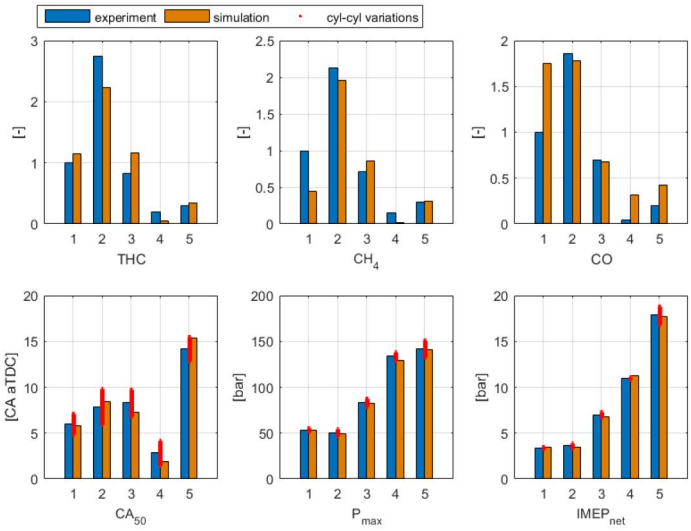

Fig. 6: Validation results for engine B. Engine control related parameters and emissions - model (brick) vs experiment (blue), for a combined load and BR sweep. Error bars indicate mean cylinder-to-cylinder variations. Emission values are relative to the experimental value of case 1 [30].

For the current study, the validated model is fed with detailed geometry of the MAN engine (Table 2, engine A). It is assumed that since the model is physics-based, its veracity in terms of heat release rate and resulting indicated efficiency (the study's focus) is maintained on a new geometry. Appendix B provides justification of this assumption and results of the functionality check performed on the scaled-up model.

3.3 Scope and workflow of RCCI simulations

Previous studies by the authors [28-30] gave an insight into the key parameters that influence efficiency and emissions of a NG-diesel RCCI engine. Amongst them, the T_{IVC}, the air-fuel equivalence ratio (λ), the SOI and the BR showed dominating effects. For each of the characteristic engine-load points (25% to 100% load), the above parameters are swept in combination with each other. The range of sweeps is based on TNO's experience with RCCI systems, which suggests a focus on high-λ operation, elevated intake temperatures and BR increasing towards high-load points. On top of that, the use of (uncooled) EGR allows extending the upper limits in T_{IVC} while sacrificing achievable λ. Hot EGR strategies have proven effective in reducing CH_4 emission at low engine-loads [31,40]. At the same time, excessive peak pressures, which prove to be the main issue for efficient high-load RCCI operation, can be reined back by applying cold EGR. These considerations have guided the design of simulations for three air-path control strategies: lean-burn RCCI strategy without EGR; with light (20%) EGR; with heavy (40%) EGR.

The experimental matrix for this study consists of 5670 simulation cases. Table 4 shows the scope of the simulations, covering all three strategies and four load points. For computational efficiency reasons, the complete set of designed simulations was run using the XCCI model, decoupled from GT-Power (see Fig. 7). This enables easy parallelization of the simulation tasks on TNO's multi-core computation cluster.

Extremum-seeking is performed to designate the best-performing RCCI conditions. Indicated specific NO_x emissions at Tier III level (2.4 g/kWh for the adopted engine speed of 720 rpm) and P_{max} limit of 180 bar are applied as design constraints for this task.

Table 4: The full scope of XCCI model simulations; n – denotes number of points explored within the sweep range.

Load point			100%		75%		50%		25%	
Reference IMEP			20 bar		15 bar		10 bar		5 bar	
Sweep parameters		Unit	Range	n	Range	n	Range	n	Range	n
0% EGR	T_{IVC}	K	331-381	6	331-371	5	331-361	4	321-351	4
	λ	-	1.8-2.6	5	1.8-2.8	6	1.8-2.8	6	1.8-2.8	6
	BR	%	75-95	5	75-95	5	70-90	5	60-80	5
	SOI	CA bTDC	65-35	3	65-35	3	65-35	3	65-35	3
Combinations			450		450		360		360	
20% EGR	T_{IVC}	K	340-390	6	340-380	5	340-380	5	330-370	5
	λ	-	1.1-1.7	5	1.1-1.9	6	1.1-2.0	7	1.1-2.1	8
	BR	%	75-95	5	75-95	5	70-90	5	60-80	5
	SOI	CA bTDC	65-35	3	65-35	3	65-35	3	65-35	3
Combinations			450		450		525		600	
40% EGR	T_{IVC}	K	340-390	6	340-380	5	340-380	5	330-370	5
	λ	-	1.1-1.7	5	1.1-1.9	6	1.1-2.0	7	1.1-2.1	8
	BR	%	75-95	5	75-95	5	70-90	5	60-80	5
	SOI	CA bTDC	65-35	3	65-35	3	65-35	3	65-35	3
Combinations			450		450		525		600	
Total simulations			5670							

The optimized points are further re-simulated using the developed GT-Power engine model. The diesel and NG injection rates and the burn-rate, post-processed from the XCCI model results, serve as inputs for the GT-Power simulation. The VTG, the intercooler bypass, and the EGR valve positions are further co-optimized to reproduce the IVC conditions of the corresponding XCCI subcase. If the given λ/EGR/T_{IVC} conditions are not achievable with the adopted hardware, the extremum-seeking procedure is repeated with additional constraints on maximum achievable mixture strength and intake temperature for a given EGR strategy. For improved clarity, the procedure discussed above is explained in Fig. 7. As a result of this procedure, a best-performing RCCI combustion point is designated.

Note that similar optimization approaches have been applied for marine dual-fuel engines [17- 19], yet never focused on incorporating the RCCI technology. Furthermore, the in-house combustion model that is used here (multi-zone with detail chemical kinetics and inherited emissions) by necessity, is by far more detail compared to the models that were fit for the purpose of [18] (2-zone, phenomenological, no emissions) and [19] (single zone, Wiebe).

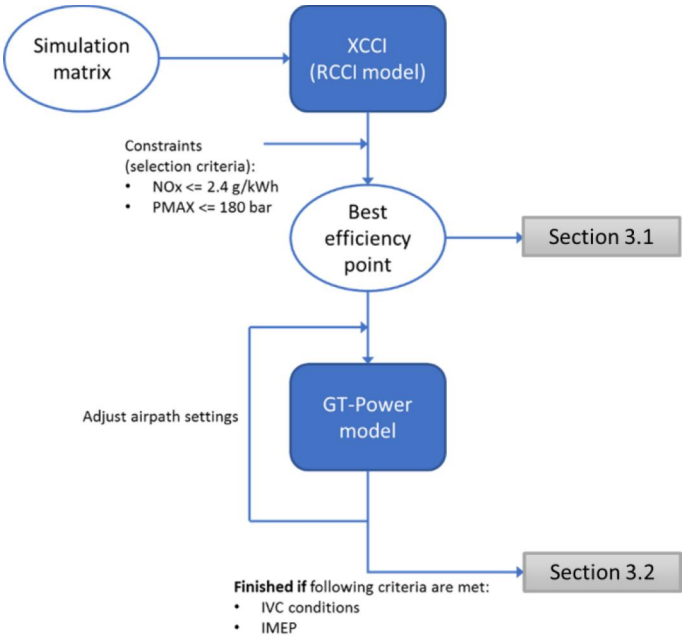

Fig. 7: Block diagram representing the simulation workflow.

2.4 Definitions and post-processing methods

In this subsection, several engineering definitions are introduced for the purpose of analyzing and discussing the simulations results in the next chapter. Note that the BR definition used consistently in this study is energy-based:

$$BR = \frac{\dot{m}_{NG} LHV_{NG}}{\dot{m}_{diesel} LHV_{diesel} + \dot{m}_{NG} LHV_{NG}} \quad (1).$$

The terms in Eq. 1 stand for mass flow rates ($\dot{m}$) and lower heating values (LHV) of NG and diesel respectively.

The raw simulation results of the XCCI model are given in terms of pressure, temperature, volume and mixture composition for each zone and at each timestep. Emissions such as NO_x and CO, in ppm (parts per million) are calculated from the zone-averaged cylinder composition at Exhaust Valve Opening. The concentrations of individual hydrocarbons and CO at this point are taken to calculate combustion efficiency. This is done with the simplifying assumption that all of the unburned HC, except the CH_4, are diesel fuel particles. Then, the combustion efficiency becomes:

$$\eta_{comb} = 1 - \frac{\dot{m}_{CH_4,res} LHV_{CH4} + \dot{m}_{CO,res} LHV_{CO} + \dot{m}_{NMHC,res} LHV_{diesel}}{\dot{m}_{diesel} LHV_{diesel} + \dot{m}_{CNG} LHV_{CNG}} \quad \#(2).$$

The $\dot{m}$ terms with subscripts: "CH_4,res", "CO,res", and "NMHC,res" represent the concentrations of the corresponding species at EVO recalculated with the total exhaust flow to the adopted convention of mass flow ([kg/s]).

HRR is calculated using a standard procedure based on the first law of thermodynamics, well described by Heywood [47]. A constant ratio of specific heats (γ=1.37) is used. The net HRR is corrected with heat transfer to the walls (calculated from the model), to give the gross HRR, which is presented in the following sections. Furthermore, the gross HRR serves as the basis for the calculation of cumulative heat release (CHR) and determination of CA10 and CA50 (crank angle at 10% and 50% heat released, respectively). The $IMEP_{gross}$ is calculated by integrating the pressure signal through the closed part of the cycle. Indicated gross efficiency is defined as:

$$\eta_{Igross} = \frac{{}^{1}/_{2} \cdot IMEP_{gross} \cdot V_{disp} \cdot N}{\dot{m}_{diesel} LHV_{diesel} + \dot{m}_{NG} LHV_{NG}} \quad (3),$$

where V_{disp} is the displacement volume and N denotes the engine rotational speed.

Air-path modelling allows the complete efficiency breakdown of the engine to be discerned at the given operating point. The direct result of the GT-Power simulation is the full-cycle, in-cylinder pressure trace calculated for each of the six cylinders. The net indicated efficiency (η_{Inet}) is calculated, from the cylinder–averaged pressure data, according to the same routine as described, for the closed part of the cycle (Eq. 3).

The pumping losses ($Pump_{loss}$) are defined as the difference between the η_{Inet} and η_{Igross}. The efficiency breakdown includes the loss of power contained in the exhaust gas exiting the system. This is calculated as an aggregated sum of all aforementioned energy streams subtracted from the total fuel energy introduced to the system (the denominator in Eq. 1, 2 and 3). The resulting exhaust losses can be written in the following form:

$$Exh_{loss} = 1 - (\eta_{Igross} + Comb_{loss} + Heat_{loss} + Pump_{loss}) \quad (4),$$

where the terms $Comb_{loss}$ and $Heat_{loss}$ denote combustion losses (defined as unity subtracted by Eq. 2) and heat losses threw cylinder walls (calculated from the instantaneous heat transfer model of XCCI) respectively.

Note that the brake efficiency is not discussed here, since the goal of the work is to assess the effect of RCCI combustion with the respect to the state-of-the art hardware. With the same hardware and same p-max constraints, the overall friction losses of the baseline LBDF platform and its RCCI twin are considered very similar.

3. RESULTS AND DISCUSSION

The discussion of the results follows the structure of the diagram in Fig. 7. First, the efficiency maps resulting from the XCCI combustion simulations are discussed along with the considered NO_x emission, peak pressure and air-path (λ / EGR / T_{IVC}) constraints. This is done for selected operating points to identify favourable conditions for RCCI combustion on large-bore engines. Next, in subsection 3.2, the optimized RCCI operating points are discussed and assessed against the baseline LBDF combustion concept. This part of the discussion is focused on efficiency and identifying the associated energy losses. The 75% load point (without EGR) is selected for detail analysis because it is frequently used in an off-shore ship operational profile [48]. This point serves as a basis for exploring efficiency improvement measures, discussed in subsection 3.3.

3.1 Efficiency maps and operational constraints

This subsection discusses the optimization space of the simulated engine at a representative operating point. All results for the given load/EGR point (Table 4) are presented in the form of maps of parameters relevant for the purpose of the present study. This includes η_{Igross} as an optimized parameter and the peak pressure with NO_x emissions as optimization constraints. Each of the indicators is mapped in terms of the optimization variables, separately for the ones that are air-path (λ, T_{IVC}) and fuel-path related. Due to a large amount of data, the discussion is based on the results of the 75% load case. Note that the optimization results for the other operating points are included in Appendix C. The discussion is supplemented by remarks on operating constraints resulting from the adopted engine air-path configuration.

The maps for the 75% load operating point, for both the non-EGR and 20% EGR RCCI cases, are presented in Figures 8 and 9 respectively.

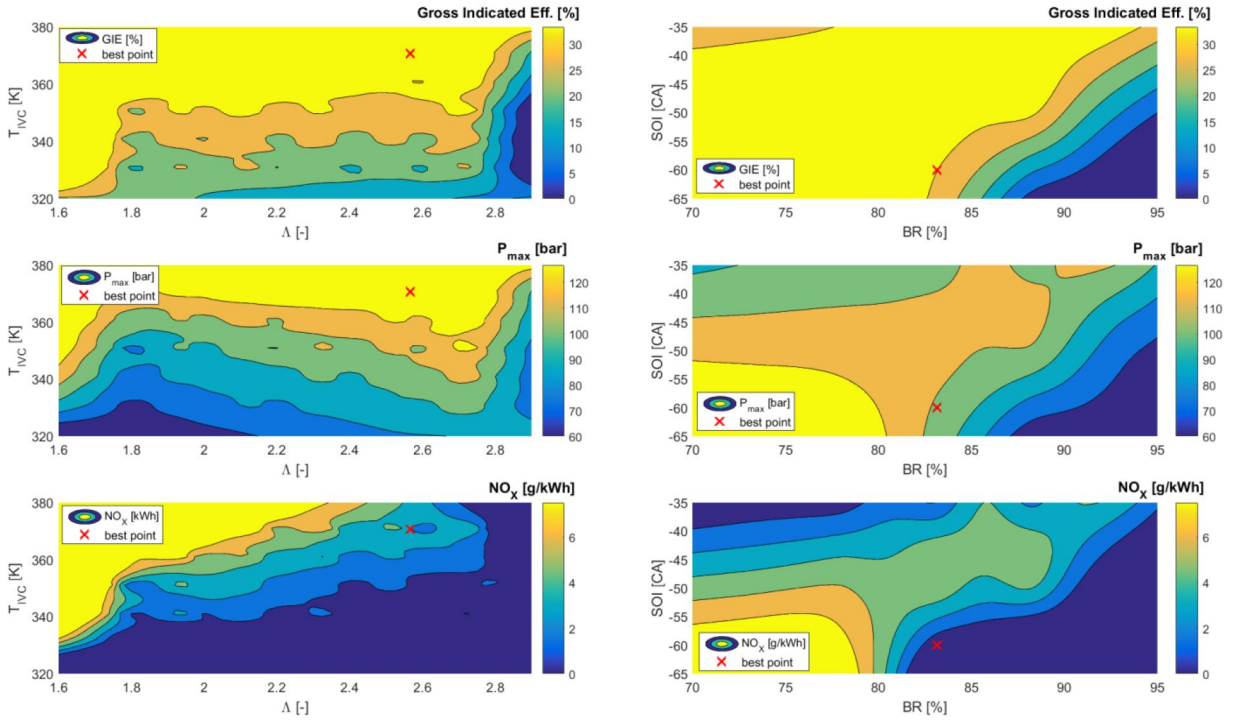

Fig. 8: Efficiency, peak pressure and NO_x emissions for the 75% load / no-EGR case mapped on the optimization parameters matrix. The left and right plots show the maps with respect to the air-path and fuel-path variables respectively.

One can observe from Fig. 8 that the contour areas of indicated efficiency do not cover values exceeding 35%. Note that the actual efficiencies of the optimized points are significantly higher (see Fig. 11 in subsection 3.2). However, since the optimization relies on a multidimensional matrix of variables, each point of the individual map is actually an average of multiple points with different performances. To be exact, for a given value of λ and T_{IVC} this is the average of points with different BR and SOI. Thus, the efficiency values in Figures 8 and 9 highlight the areas of the map where the results of RCCI combustion generally tend to show increased performance. The same applies to the maps of the peak pressure and NO_x emissions.

Considering the above remarks, the best efficiencies for RCCI are achieved for high T_{IVC} and early injection timings with energy-based diesel content around 20%, as evident from Fig. 8. However, the peak pressure and NO_x emissions also tend to maximize in the same region, indicating a strong trade-off relationship. On the other hand, the best point within the adopted NO_x and P_{max} limit is, at the same time, the global efficiency optimum. This shows that the optimization is not constrained by the adopted limits. Note that this is not the case for the full load, for which the simulation results indicate very high values of peak pressures achieved over the whole optimization space (Fig. A3). On the contrary, for the low-load operation (Fig. A4) the maximum attainable pressures are not exceeding 80 bar for any investigated point and the high NO_x emission regions do not overlap with high-efficiency regions. Note however that the gross indicated efficiencies are lower, compared to the high-load points. This is discussed in more detail in subsection 3.2.

Figure 9 shows the maps for the 75% load point with 20% EGR. The EGR addition extends the high-efficiency area. At the same time, however, the high NO_x and peak pressure regions extend significantly. Additionally, the global best-case scenario with EGR results in around 0.25 percentage point lower indicated efficiency compared to the best efficiency case without EGR, due to slower combustion.

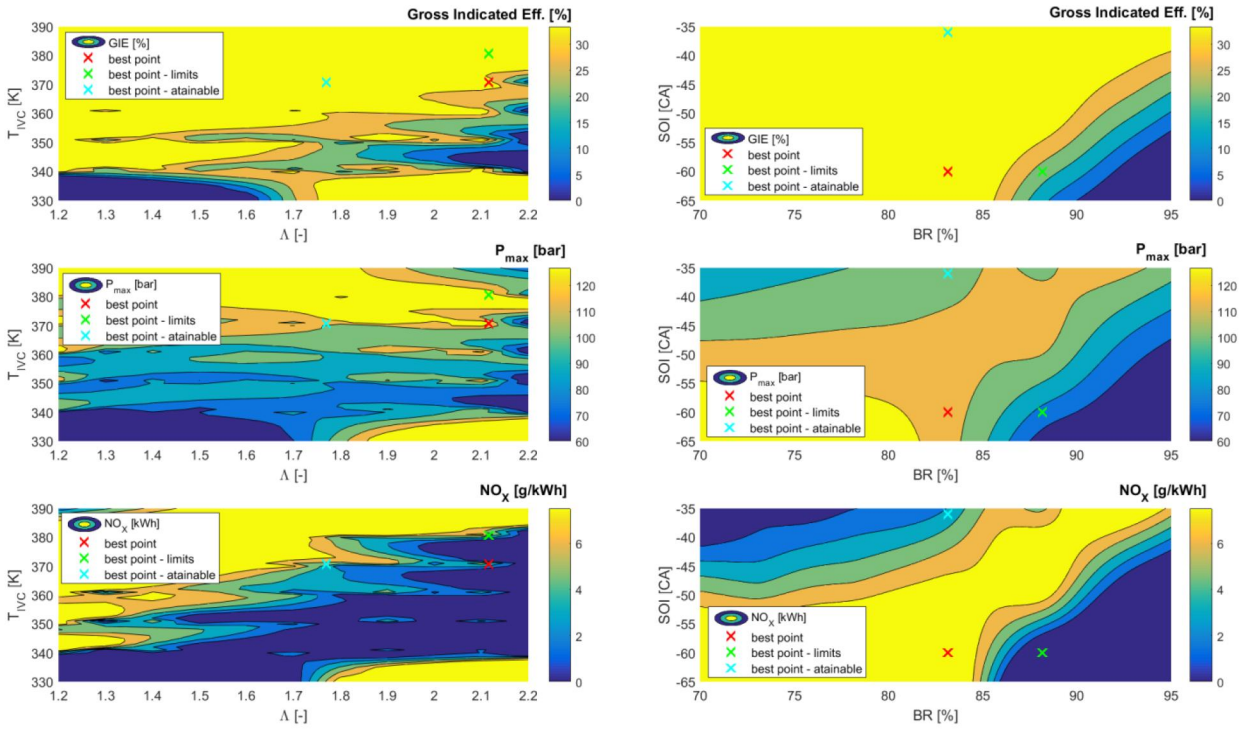

Fig. 9: Efficiency, peak pressure and NO_x *emissions for the 75% load / 20%-EGR case mapped on the optimization parameters matrix. The left and right plots show the maps with respect to the air-path and fuel-path variables respectively.*

The highest efficiency is attained with high EGR percentage and high λ. This, however presents the challenge for the air-path. In order to explore the boundaries of maximum achievable EGR ratio, within the constraints of λ, GT-Power simulations are performed. This involves scaling of the maps for the turbine and compressor, followed by a sweep on the VTG position. Figure 10 shows the variation of λ and EGR (internal and external) as a function of VTG position. It is clear from that figure, that the maximum achievable EGR ratio, for the 19 Bar IMEP point, is only 20%, if the λ constraint of 1.5 is to be maintained. For the 16 bar IMEP point, the situation is similar. The only feasible point is at the VTG position of 0.6, which corresponds to a global λ of 1.9 and EGR ratio of 22%.

The best efficiency point meeting both NO_x and P_{max} constraints, after including the turbocharger hardware limits, is marked in Figure 9 (75% load / 20% EGR) by the cyan cross. The maximum EGR ratio attainable for RCCI operation, with the stock turbocharger configuration, while having a reasonably high λ, is 20%. Under such conditions, it is not possible to achieve higher efficiencies or lower emissions compared to the non-EGR strategy. For this reason, the 40% EGR strategy explored in the XCCI simulations is considered unrealizable with the discussed hardware and consequently, is not further evaluated with GT-Power in the present study. Finally, note that the adopted T_{IVC} and λ ranges, for all non-EGR RCCI load cases, are achievable with the current hardware setup.

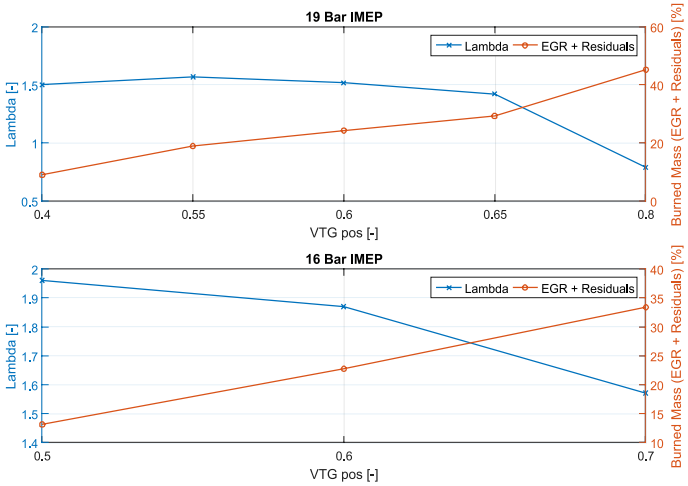

Fig. 10: λ and EGR + Residuals for 19 Bar IMEP and 16 Bar IMEP as a function of VTG position.

3.2 Best efficiency points for stock hardware configuration

This subsection discusses in more detail the results of the optimization procedure applied to the XCCI simulation outputs, according to the workflow presented in Figure 7. The selected RCCI points, constrained by indicated efficiency-optimized and peak-pressure/emissions, have been simulated with GT-Power to provide full energy breakdown analysis. The operating conditions associated with the cases discussed in this chapter are highlighted in Table 5.

Table 5: Basic operating conditions for the optimized cases discussed in this chapter.

Load point	Case no.	Case description	T_{IVC} [K]	λ [-]	SOI [CA] bTDC	BR [%]
100%	1	no EGR	381	2.2	-38	93
	2	no EGR ↑ P_{max}	371	2.4	-60	88
	3	20% EGR	371	1.6	-36	78
75%	4	no EGR	371	2.6	-60	83
	5	20% EGR	371	1.8	-36	83
50%	6	no EGR	361	2.8	-60	73
25%	7	no EGR	351	2.6	-60	58
	8*	20% EGR	371	2.5	-60	58
	9*	40% EGR	381	2.2	-60	58
* XCCI results only - not re-simulated in GT-Power						

The results of optimizing RCCI operation for different engine load demands and different strategies are summarized in Figures 11 and 12. Figure 11 presents the results in terms of efficiency breakdown (eq. 2-4) including pumping, heat transfer and combustion losses. It is clear that the RCCI concept has the best indicated efficiency point at 75% load. For the non-EGR case, gross efficiency reaches 48.4% (sum of indicated net efficiency and pumping losses). At this point, the optimal combustion phasing is not heavily constrained by excessive peak pressure, which is the case for full-load operation. At the same time, high T_{IVC} and high turbulence, invoked by the boosted operation, support good combustion efficiencies. Lowering both those parameters, by the necessity of keeping the air-path constraints (T_{IVC}) and proper λ (boost pressure), limits the combustion propagation and thus negatively affects combustion efficiency at lower engine-loads. Combustion efficiency decreases consistently with engine-load, from almost 98.8% through 96.3% to only 91.2% respectively for engine loads of 75%, 50% and 25%. Table 5 shows that the lower-load cases optimize for significantly lower blend ratios. This is the manifestation of the optimizer attempting to reach better combustion efficiency. The low BR (i.e. more diesel) increases global mixture reactivity, supporting

more complete combustion. These results confirm that the typical issues arising in partial-load RCCI in heavy-duty engines [31] are also present in large-bore systems.

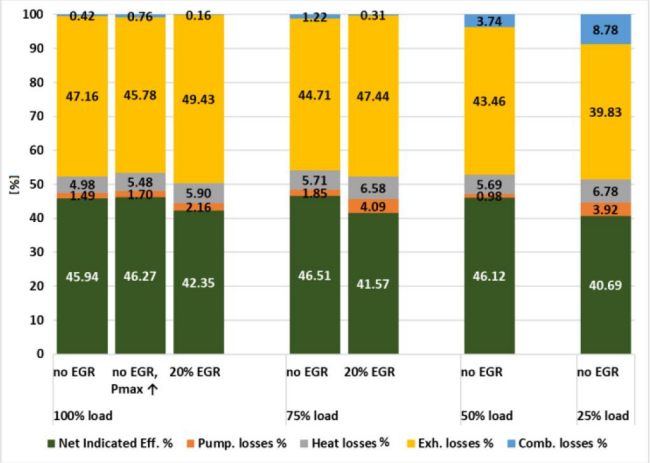

Fig. 11: Full efficiency breakdown analysis (including friction,) for best-performing RCCI points, across typical load conditions. Stock hardware.

For the base RCCI case at full load (case 1), the gross indicated efficiency is 47.4% which is 0.9 percentage point lower than the lean 75% load case (case 4). Note that this is despite combustion efficiency improving as engine-load increases. This suggests that the combustion phasing is not optimal (compare with Fig. 13), while the engine is operating in RCCI mode at full load. Confirmation of this observation can be found in a comparison of the exhaust losses, which are significantly larger in case 1 than in case 4. Note that, in terms of net indicated efficiency, the result of 100%-load base RCCI case is similar to the baseline LBDF concept re-simulated with GT-Power. If peak pressure constraint is relaxed (Fig. 11, elevated P_{max}), higher λ is attainable (Table 5) and better combustion phasing is realized (Fig. 11). Together, they contribute to lower exhaust losses and thus higher η_{Igross} of 48%.

Introducing EGR does not allow better RCCI efficiency at high load (see Fig. 11, 20% EGR case). The suspected advantages of reduced peak pressures and NO_x emission levels, giving theoretically wider efficiency optimization potential, are not confirmed in this study. The optimized EGR operating point is at a low λ of 1.63, due to air-path limitations. At the same time, late injection and low BR (73%) are necessary to keep proper combustion phasing and P_{max} within design limits (Fig. 13). Exhaust losses are particularly high for the high-load EGR strategy, resulting in 44.51% and 42.35% gross and net indicated efficiently respectively.

The trends in combustion efficiency manifesting in Fig. 11 are confirmed in the results of THC emissions presented in Fig. 12. The main challenge for LBDF when facing Stage V legislation lies in HC and CO emissions, but Fig. 12 shows high-load RCCI is realizable with ultra-low THC and CO emissions. Note that the model does not take the crevice volume explicitly into account, and in reality, emissions of both compounds can be slightly higher. The author's experience with RCCI suggests achieving high-load THC emissions lower than 1 g/kWh is hardly possible. Nevertheless, the conclusion to be taken from the results illustrated in Fig. 12 is that lean RCCI combustion strategy for high loads in mid-speed engines has the potential to meet Stage V emission limits. Note that for 100% and 75% loads this particular realization of RCCI allows for further THC emission reduction if EGR is employed. This comes at the expense of greater CO emissions, hindering overall emission reduction potential.

Figure 12 illustrates that THC and CO emissions become increasingly challenging for RCCI as engine-load is reduced. THC emission for the 25%-load case is excessive and over 18g/kWh. The 50%-load RCCI case, however, still exhibits lower THC and CO emissions than the reference, high-load LBDF case. In terms of NO_x, the results are in all cases below the Tier III limits. Achieving a further reduction of NO_x, towards Stage V level, should be possible for RCCI without a large efficiency penalty.

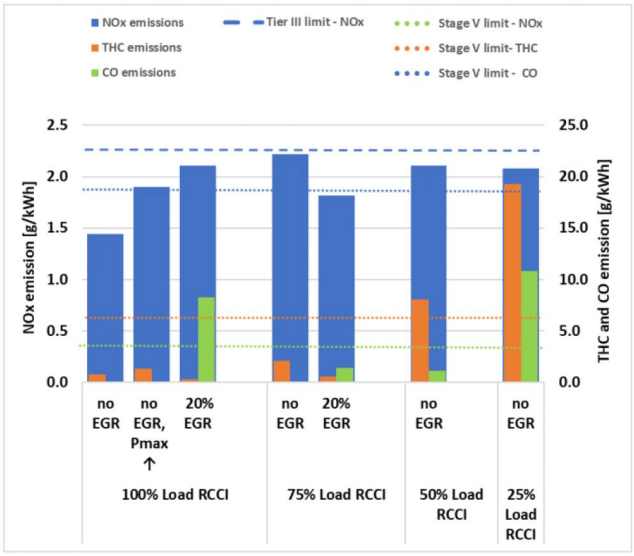

Fig. 12: Engine-out emissions (THC, NO_x and CO) results for all the discussed points. Tier III limit (NO_x) is indicated as dashed line and Stage V limits are indicated as dotted lines respectively for each compound.

Figure 13 provides additional information on the combustion phasing, combustion duration and peak pressure, supporting the statements about the indicated efficiency results. The CA50 retards from the optimal setpoint (around TDC) for all full-load RCCI cases in order to mitigate excessive peak pressures. Allowing for higher P_{max} already reduces the CA50 from 12.2 CA to 6.1 CA aTDC. This, more optimal, combustion phasing explains the 0.7 percentage point increase in indicated efficiency for the elevated P_{max} strategy over the baseline RCCI. Note that combustion duration (Fig. 13), mixture strength (Table 5), and combustion efficiencies (Fig. 11) are similar in both cases. This effect is escalated at 75% load, where the P_{max} is not constraining the ability to optimize for combustion phasing (the best efficiency point under constraints is also the global optimum for the given configuration). At this load point, the CA50 value is close to its optimum at TDC and the combustion duration (defined here as the distance between CA05 and CA50) reaches saturation at around 25 CA – similarly for the optimum 100%-load points. Fast combustion supports achieving higher indicated efficiency. Furthermore, the combustion duration seems to be the minimum attainable for the RCCI combustion with the considered large-bore engine hardware setup. Note that both addition of EGR and reduction of engine load below 75% elongate the combustion duration. This is because EGR reduces mixture reactivity, while lower engine loads are associated with lower boost pressures and hence less in-cylinder turbulence.

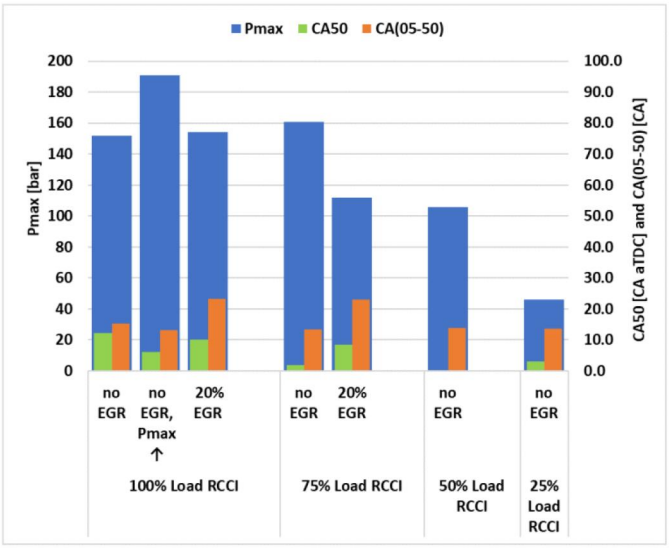

Fig. 13: Combustion indicators: CA50 combustion duration (CA05-CA50) and peak pressure, for all the discussed points.

Despite EGR failing to improve RCCI performance at high loads, the simulation results show considerable benefits for EGR at lower engine loads. Figure 14 focuses on the 25%-load case, comparing results without EGR, with 20% EGR and with 40% EGR. These cases are not simulated in GT-Power, so only gross indicated efficiencies are provided to give a broad view of the potential of hot EGR-based RCCI for low-load operation.

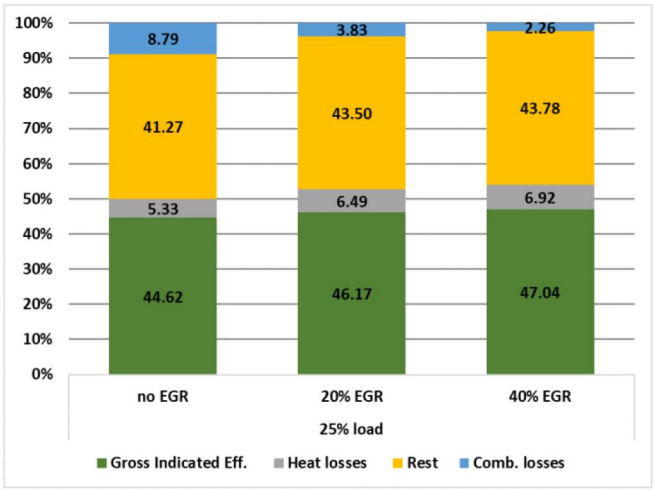

Fig. 14: Efficiency breakdown for 25% load cases. Note that the EGR realizations are not simulated in GT-power, thus the breakdown includes only the results of the closed part of the cycle.

Figure 14 shows that adding even mild EGR reduces combustion losses by more than half, giving a 1.5 percentage point indicated efficiency improvement. The effect is reinforced with the heavy EGR strategy. The combustion efficiency improvement comes from: (i) increased T_{IVC} (see Table 5), (ii) reintroduction of unburned hydrocarbons to the cylinder. For the second mechanism, the EGR contains some reformed hydrocarbons (like aldehydes) which have additional combustion-promoting effects [49]. Note, that the efficiency improvement can be attained if sufficiently high λ can be maintained while EGR is introduced (Table 5).

3.3 Efficiency improvement potential with hardware changes

All the above results come from employing RCCI on stock hardware, with or without optional EGR. This section discusses how changes to the basic hardware can further improve the considered large-bore RCCI engine platform. In search of brevity, this is examined in detail for only one of the basic measures: optimization of compression ratio. Other more sophisticated RCCI improvement measures are mentioned in brief.

3.3.1 Compression ratio optimization

The benefits of introducing higher (diesel-like) CR for improving NG-diesel RCCI performance were reported by Splitter et al. [50]. The maximum attainable theoretical efficiency of the engine cycle depends directly on CR and mixture strength. Furthermore, higher CR produces higher compression temperatures and pressures, supporting faster and more complete RCCI combustion [50]. The baseline engine (Engine A) has a low CR of 12.2:1, imposed by the characteristics of LBDF combustion where λ is limited (maximum λ around 2) by misfire limit. At such mixture strengths and high BR (necessary to reduce NO_x), the CR has to be lowered to avoid knock [51]. In RCCI, with lower BR and higher intake temperatures the misfire limit is by far extended, and the efficiency optimizes for much leaner mixtures (Table 5 - λ between 2.3 and 2.6, depending on the operating point). This enables higher CR if the engine was designed explicitly for RCCI. Note that TNO has successfully demonstrated full-load, NG-diesel RCCI on a heavy-duty platform with geometrical CR of 14:1 [28].

Figure 15 shows how changing the geometrical CR in the discussed large-bore engine effects RCCI performance at the previously optimized 75% load point. Black circles represent a “clean” (no other parameter was changed) CR sweep from the baseline CR of 12.2 to 15.2. It is evident that elevating the CR has a positive impact on both indicated and combustion efficiency, implying lower HC and CO emissions. Note, however, that the indicated efficiency improvement potential is hindered by changes in combustion phasing. The CA50 is shifted before TDC, imposing additional work on the piston during compression and thus limiting the effective work and contributing to excessive peak pressures. In this case, the shift in CA50 results mainly from the over-accelerated start of combustion, which can be mitigated by engine measures. From the results of the sensitivity analysis (Appendix D), one can see that especially elevating the BR (Fig. A7) and lowering TIVC (Fig. A5) can be used to retard the combustion phasing. Both strategies are beneficial for mitigating NO_x, which tends to increase significantly with elevated CR (Fig. 15). Additionally, a higher BR means less diesel consumption and so is favourable from an economic perspective.

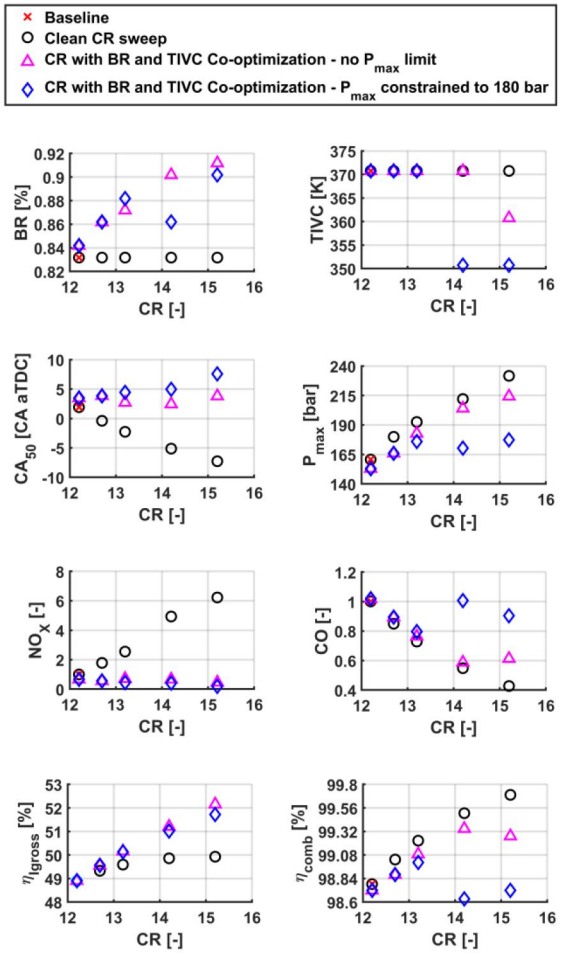

Fig. 15: Black Circles – clean CR sweep, red X – CR with BR and T_{IVC} co-optimization – no P_{max} limit; blue diamonds – CR with BR and T_{IVC} co-optimization – P_{max} constrained. NO_x and CO emissions are scaled such that baseline point = 1.

Taking the above into account, the results of optimizing the CR together with the BR and T_{IVC} are shown in Fig. 15 by red crosses. This refers to the results with no additional constraints on peak pressure or NO_x emissions. One can note, that the almost linear trend in indicated efficiency can be maintained for the explored CR range. A superior 52.2% gross indicated efficiency can be obtained for CR of 15.2. Figure 15 reveals that this is attained mainly by keeping the combustion phasing close to the optimized setpoint. Note, that the proper combustion phasing is assured with increasing the BR while maintaining the T_{IVC} as high as possible. When the BR reaches around 92%, further increasing it results in a rapid drop in combustion efficiency, despite the CR increase. Thus, beyond this point, the T_{IVC} is reduced to keep the phasing in line. Importantly, the BR increase deals with the NO_x emissions, which is evident from Fig. 15. Although optimizing the BR and TIVC to some extent hinders the peak pressure increase associated with a higher CR, the imposed P_{max} limit is still exceeded if CR goes beyond 13.2.

Blue diamonds in Fig. 15 indicate the best efficiencies achieved for various CRs while imposing additional peak pressure constraint on the optimization. Note, that achieving 51.8% gross indicated efficiency with CR=15.2 while keeping the P_{max} below 180 bar is possible. This is achieved by balancing the CR effect with both BR and T_{IVC}, allowing for slightly retarded combustion (consult CA50 plot in Figure 15). In this case, any combustion efficiency gain caused by higher CR is hindered by lowering the temperature. Indicated specific CO emissions are slightly reduced compared to the base case but this mainly results from higher efficiency and not from reduced CO concentrations in the exhaust.

3.3.2 Other potential efficiency improvement measures

Summarizing the findings on CR adjustment, optimum RCCI combustion with high efficiency and low emissions (NO_x, THC, and CO) is achieved by operating lean, yet taking care that no over-dilution takes place. Proper combustion phasing should be maintained by sufficiently high T_{IVC} and optimizing BR. The CR can be increased for partial loads to elevate the end-compression temperature and to speed up combustion. Both Variable Valve Actuation (VVA) and Variable Compression Ratio (VCR) technologies give the flexibility in the CR compression ratio by either changing the geometrical value of this parameter. Alternatively, using the Miller cycle is another option, providing there is sufficient boost reserve. For detail discussion on the effect of different VVA strategies on RCCI combustion, see the work by Mikulski et al. [31].

Previous research has shown that RCCI efficiency is largely dependent on the in-cylinder turbulence level [30, 31, 52]. Higher turbulence supports faster mass transfer from the igniting, diesel-rich regions to less reactive areas. As a result of the combustion, initiating near the cylinder walls is generally faster and is able to propagate further into the inner parts of the cylinder, which have the lowest reactivity. Both the shorter and the more complete combustion are conducive to higher indicated efficiencies. Simulation results regarding turbulence effect on the 75%-load point are presented in appendix D. In-cylinder turbulence can be enhanced by design (intake port/valve and combustion chamber redesigning [53]) or via adjustable measures like variable intake valve opening [31].

The local reactivity gradient of RCCI can be influenced by changing the BR and diesel injection parameters. Introducing direct injection of natural gas instead of the standard PFI system would allow additional control by means of low-reactivity fuel stratification. A simulation study by Mikulski and Bekdemir [30] showed that considerable benefits can be attained for low-load RCCI efficiency if natural gas is highly stratified in the cylinder, but the strategy has not yet been experimentally demonstrated.

Finally, the reactivity of the fuel mixture can be globally changed to improve combustion efficiency. This can be done by either pre-blending natural gas with other, more reactive gasses (ethane) or by introducing onboard fuel-reactivity enhancement techniques, such as external fuel reformers [54]. Alternatively, fuel reforming can be achieved in the recompressed exhaust gases during negative valve overlap [55]. To this end, VVA is used to switch between negative and positive overlap, depending on the operating point.

All these measures (VVA/VCR, direct injection of low reactive fuel or fuel reforming) add considerable complexity and cost. Another option may be to combine multiple combustion concepts. If keeping geometrical CR at a moderate level it might be possible to use LBDF for the lower part of the operating range (CR would be on the high end with good efficiency) and employ RCCI for the high end (CR would be low enough to allow high λ without exceeding maximum pressure constraints). Another interesting mode-switching alternative is to combine the benefits of RCCI at partial loads with HPDI (gas-diesel) combustion mode for reducing methane slip at low loads. A feasible method for RCCI mode switching control has been demonstrated by Indrajuana et al. [39].

4. CONCLUSIONS

This study assesses the feasibility of Natural Gas – Diesel RCCI combustion as a potential solution for next-generation marine engines. This is done by simulating the concept's performance on the 350 mm bore, mid-speed engine platform. The simulation applied an engine hardware configuration similar to the one used for so-called Lean-Burn Dual Fuel (LBDF) combustion, one of the current solutions that meet the IMO Tier III emission regulations. The conclusions are as follows:

Lean RCCI is achievable with the current dual-fuel engine hardware. The operation is not limited by attainable λ or IVC temperature. Emissions are within the IMO Tier III emission limits and efficiency under high-load conditions is similar to the reference LBDF combustion. Best RCCI efficiency is demonstrated at 75 % load, where high (close to 99%) combustion efficiency can be achieved and excessive peak pressures do not limit the optimization regime. Simulated net indicated efficiency is 46.5% at this point.

Using the existing engine hardware, RCCI's advantage over the baseline LBDF concept is lower CH_4 and CO emissions at high loads, potentially allowing it to meet the rigorous European Stage V legislation for inland waterway

vessels. The disadvantage is the need to keep the Blend Rate at 80%-90% compared to LBDF's 95%-99%. With current prices of natural gas and diesel, this makes LBDF beneficial in terms of operational costs.

The simulation results confirm that RCCI's poor combustion efficiency at low loads, previously noted in studies with a heavy-duty truck engine, is also evident in the considered large-bore engine. At 25% load, increasing the combustion efficiency beyond 92% is not possible with the stock engine hardware. Employing hot EGR, combined with relatively lean mixtures, can solve this problem. However, this strategy failed to provide any benefits for high-load operation, mainly due to the limitations of the stock turbocharger. The most reasonable λ/EGR tradeoff realized at 100% load is 1.6 and 20% respectively. Although giving small benefits in combustion efficiency, this strategy suffers from lower indicated efficiency and increased pumping losses.

The study confirmed the ability of an RCCI large-bore platform to run at much leaner mixtures compared to LBDF without hitting the misfire limit. This allows a higher compression ratio without risk of knocking. It is shown that the optimized mid-speed RCCI engine, with a compression rate of 15.2, can deliver gross indicated efficiencies in the range of 52% while preserving the advantages of high blend rate (over 90%) and achieving NO_x, CH_4 and CO emissions below the rigorous Stage V level.

The above intermediate conclusions allow the authors to answer the main research question of the study by stating that natural gas–diesel RCCI combustion is a feasible, short-term alternative for clean and efficient maritime propulsion. According to simulation results, as a first-stage improvement, RCCI can be implemented as a mode-switching solution on existing mid-speed engine platforms without any hardware changes.

NOMENCLATURE

$\dot{m}$	Mass Flow Rate
η	Efficiency: I – Indicated (Gross Or Net), Comb – Combustion
λ	Air-Fuel Equivalence Ratio
aTDC / bTDC	After / Before Top Dead Center
BR	Blend Rate
CA	Crank Angle
CAXX	Crank Angle at XX% Heat Released [CA]
CDF	Conventional Dual Fuel
CH_4	Methane
CHR	Cumulative Heat Release
CI	Compression Ignition
CO	Carbon Monoxide
CO_2	Carbon Dioxide
CR	Compression Ratio
Ct	Turbulent Mixing Coefficient
DF	Dual-Fuel
DICI	Direct Injection Compression Ignition
ECA	Emission Control Area
EGR	Exhaust Gas Recirculation
EVO	Exhaust Valve Opening
GD	Gasoline-Diesel
HCCI	Homogenous Charge Compression Ignition
HFO	Heavy Fuel Oil
HRR	Heat Release Rate
IMEP	Indicated Mean Effective Pressure
IMO	International Maritime Organization
LB	Lean Burn
LBDF	Lean Burn Dual Fuel
IVC	Intake Valve Closing

LNG	Liquefied Natural Gas
MGO	Marine Gas Oil
MPDF	Micro-Pilot Ignited Dual Fuel
NG	Natural Gas
NMHC	Non Methane Hydrocarbons
NO_x	Nitrous Oxides
NVO	Negative Valve Overlap
OEM	Original Equipment Manufacturer
PFI	Port Fuel Injection
PCCI	Premixed Charge Compression Ignition
PM	Particulate Matter
P_{max}	Peak In-cylinder Pressure
RCCI	Reactivity Controlled Compression Ignition
SCR	Selective Catalytic Reduction
SI	Spark Ignition
SOI	Start of Injection
SO_x	Sulphur Oxides
THC	Total Hydrocarbons
T_{IVC}	In-cylinder Charge Temperature at IVC
VCR	Variable Compression Ratio
V_{disp}	Displacement Volume
VTG	Variable Turbine Geometry
VVA	Variable Valve Actuation

ACKNOWLEDGMENTS

The results are part of an internal TNO project founded by the “Green Maritime Performance” PMC of TNO.

The authors would like to thank Praveen Ramanujam Balakrishnan (TNO Powertrains) for his assistance with making the figures and formatting the manuscript.

REFERENCES

[1] IMO - The 2020 global sulphur limit n.d. http://www.imo.org/en/MediaCentre/HotTopics/GHG/Documents/2020 sulphur limit FAQ 2018.pdf (accessed July 15, 2018).

[2] Hoek D. Shell: IMO2020 Readiness—Fuels and Lubricants, Delft: Alternative Maritime Fuels and Ship Emissions Seminar; 2018.

[3] EU. Regulation (EU) 2016/1628 of the European Parliament and of the Council of 14 September 2016 on requirements relating to gaseous and particulate pollutant emission limits and type-approval for internal combustion engines for non-road mobile machinery, amending Regulations (EU) No 1024/2012 and (EU) No 167/2013, and amending and repealing Directive 97/68/EC (Text with EEA relevance). Official Journal of the European Union 2016;59. https://eur-lex.europa.eu/legal-content/EN/TXT/PDF/?uri=CELEX:32016R1628&qid=1524555867189&from=EN.

[4] Emission Standards: China: Marine Engines.. https://www.dieselnet.com/standards/cn/marine.php (accessed September 14, 2018).

[5] Wärtsilä, Power Plants Solutions 2016. https://cdn.wartsila.com/docs/default-source/power-plants-documents/ppscatalog_lowres_030616_56mt.pdf?sfvrsn=e5b3dc45_2

[6] Bergen B35:40L gas engine – Rolls-Royce 2017. https://www.rolls-royce.com/products-and-services/marine/product-finder/propulsion-engines/propulsion-gas-engines/bergen-b3540l-gas-engine.aspx#section-key-technical-information (accessed May 19, 2018).

[7] Toulson E, Schock HJ, Attard WP. A Review of Pre-Chamber Initiated Jet Ignition Combustion Systems, 2010. doi:10.4271/2010-01-2263.

[8] Hummerfelt, T., Johannessen, E., Vaktskjold, E., Skarbø LA. Development of The Rolls-Royce C26:33 Marine Gas Engine Series. CIMAC Congress, Bergen, Norway: 2010.

[9] Cho HM, He BQ. Spark ignition natural gas engines-A review. Energy Conversion and Management 2007;48:608–18. doi:10.1016/j.enconman.2006.05.023.

[10] Shah A. Improving the Efficiency of Gas Engines using Pre-chamber Ignition. Lund University, 2015. http://portal.research.lu.se/portal/en/publications/improving-the-efficiency-of-gas-engines-using-prechamber-ignition(53d0741e-449c-4f9a-b2e8-6d34d80febf4)/export.html#export.

[11] Alger T, Gingrich J, Roberts C, Mangold B, Sellnau M. A High-Energy Continuous Discharge Ignition System for Dilute Engine Applications, 2013. doi:10.4271/2013-01-1628.

[12] Wei L, Geng P. A review on natural gas/diesel dual fuel combustion, emissions and performance. Fuel Processing Technology 2016;142:264–78. doi:10.1016/j.fuproc.2015.09.018.

[13] Goto S, Nishi Y, Nakayama S. High Density Gas Engine With Micro Pilot Compression Ignition Method. Design, Application, Performance and Emissions of Modern Internal Combustion Engine Systems and Components, ASME; 2003, p. 707–12. doi:10.1115/ICES2003-0679.

[14] Four Stroke 35/44DF - Profile 2017. https://marine.man-es.com/four-stroke/engines/l35-44df (accessed May 14, 2018).

[15] Janne Klemola. Completing the fuel flexible engine portfolio. Indetail, Wärtsilä Technical Journal 2010. http://twentyfour7.studio.crasman.fi/pub/web/pdf/magazine+pdfs/ID0110-WWW-HQ.pdf (accessed May 24, 2018).

[16] Wang B, Li T, Ge L, Ogawa H. Optimization of combustion chamber geometry for natural gas 587 engines with diesel micro-pilot-induced ignition. Energy Conversion and Management, 2016, 122, 552-563. 588 http://dx.doi.org/10.1016/j.enconman.2016.06.027

[17] Mavrelos C & Theotokatos G. Numerical Investigation of a Premixed Combustion Large Marine Two-Stroke Dual Fuel Engine for Optimising Engine Settings via Parametric Runs. Energy Conversion and Management. 2018 .

[18] Sixel EJ, Hiltner J, Rickert C. Use of 1-D simulation tools with a physical combustion model for the development of Diesel-Gas or Dual Fuel engines, PAPER NO.: 124. 28th CIMAC World Congress 2016. Helsinki.

[19] Stoumpos S, Theotokatos G, Boulougouris E, Vassalos D, Lazakis L, Livanos G. Marine dual fuel engine modelling and parametric investigation of engine settings effect on performance-emissions trade-offs, Ocean Engineering; 2018, 157, p. 376-386. doi: 10.1016/j.oceaneng.2018.03.059.

[20] Besch MC, Israel J, Thiruvengadam A, Kappanna H, Carder D. Emissions Characterization from Different Technology Heavy-Duty Engines Retrofitted for CNG/Diesel Dual-Fuel Operation. SAE International Journal of Engines 2015;8:2015-01-1085. doi:10.4271/2015-01-1085.

[21] McTaggart-Cowan G, Mann K, Wu N, Munshi S. An Efficient Direct-Injection of Natural Gas Engine for Heavy Duty Vehicles, 2014. doi:10.4271/2014-01-1332.

[22] Ouelette P, Goudie D, McTaggart-Cowan G. Progress in the development of natural gas high pressure direct injection for Euro VI heavy-duty trucks, Springer Vieweg, Wiesbaden; 2016, p. 591–607.

[23] McTaggart-Cowan G, Mann K, Huang J, Singh A, Patychuk B, Zheng ZX, et al. Direct Injection of Natural Gas at up to 600 Bar in a Pilot-Ignited Heavy-Duty Engine. SAE International Journal of Engines 2015;8:2015-01–0865. doi:10.4271/2015-01-0865.

[24] Arnberger A, Golini S, Mumford D, Hasenbichler G. Commercial natural gas vehicles: tomorrow's engine technologies for most stringent NO_x and CO2 targets, Springer Vieweg, Wiesbaden; 2018, p. 315–38. doi:10.1007/978-3-658-21015-1_21.

[25] Portin K. Wärtsilä Duel Fuel (DF) Engines for Offshore Applications and Mechanical Drive. 26th CIMAC World Congress on Combustion Engine Technology, Bergen, Norway: 2010.

[26] ME-GI Dual Fuel MAN B&W Engines: A Technical, Operational and Cost-effective Solution for Ships Fuelled by Gas n.d. https://www.corporate.man.eu/man/media/content_medien/doc/global_corporate_website_1/verantwortung_1/megatrends_2/klimawandel/me_gi_dual_fuel_en_01.pdf (accessed May 14, 2018).

[27] Reitz RD, Duraisamy G. Review of high efficiency and clean reactivity controlled compression ignition (RCCI) combustion in internal combustion engines. Progress in Energy and Combustion Science. 2015;46:12–71. doi:10.1016/j.pecs.2014.05.003.

[28] Doosje E, Willems F, Baert R. Experimental Demonstration of RCCI in Heavy-Duty Engines using Diesel and Natural Gas, 2014. doi:10.4271/2014-01-1318.

[29] Mikulski M, Bekdemir C, Willems F. Experimental validation of a combustion kinetics based multi-zone model for natural gas-diesel RCCI engines. Symposium for Combustion Controll, Aachen, Germany: 2016.

[30] Mikulski M, Bekdemir C. Understanding the role of low reactivity fuel stratification in a dual fuel RCCI engine – A simulation study. Applied Energy 2017;191:689–708. doi:10.1016/j.apenergy.2017.01.080.

[31] Mikulski M, Balakrishnan PR, Doosje E, Bekdemir C. Variable Valve Actuation Strategies for Better Efficiency Load Range and Thermal Management in an RCCI Engine, 2018. doi:10.4271/2018-01-0254.

[32] Jia Z, Denbratt I. Experimental Investigation of Natural Gas-Diesel Dual-Fuel RCCI in a Heavy-Duty Engine. SAE International Journal of Engines 2015;8:2015-01–0838. doi:10.4271/2015-01-0838.

[33] Dahodwala M, Joshi S, Koehler E, Franke M, Tomazic D. Experimental and Computational Analysis of Diesel-Natural Gas RCCI Combustion in Heavy-Duty Engines, 2015. doi:10.4271/2015-01-0849.

[34] Hanson R, Ickes A, Wallner T. Comparison of RCCI Operation with and without EGR over the Full Operating Map of a Heavy-Duty Diesel Engine, 2016. doi: 10.4271/2016-01-0794.

[35] Dempsey AB, Walker NR, Gingrich E, Reitz RD. omparison of Low Temperature Combustion Strategies for Advanced Compression Ignition Engines with a Focus on Controllability, Combustion Science and Technology, 186:2, 210-241, DOI: 10.1080/00102202.2013.858137

[36] García Valladolid P, Tunestål P, Monsalve-Serrano J, García A, Hyvönen J. Impact of diesel pilot distribution on the ignition process of a dual fuel medium speed marine engine. Energy Conversion and Management 2017;149:192–205.

[37] MAN Diesel & Turbo, MAN L35/44DF Project Guide - Marine, Four-stroke dual fuel engines compliant with IMO Tier II n.d. https://marine.man-es.com/docs/librariesprovider6/4-stroke-project-guides/man-l35-44df-imo-tier-ii-marine.pdf?sfvrsn=9397f232_17 (accessed November 14, 2018).

[38] MAN Diesel & Turbo, Exhaust Gas Turbochargers, Program 2015 n.d. https://mandieselturbo.com/docs/default-source/sales-force-package/exhaust_gas_turbocharger_program_2015.pdf?sfvrsn=4 (accessed November 14, 2018).

[39] Indrajuana A, Bekdemir C, Feru E, Willems F. Towards Model-Based Control of RCCI-CDF Mode-Switching in Dual Fuel Engines, 2018. doi:10.4271/2018-01-0263.

[40] Desantes JM, Benajes J, García A, Monsalve-Serrano J. The role of the in-cylinder gas temperature and oxygen concentration over low load reactivity controlled compression ignition combustion efficiency. Energy 2014;78:854–68. doi:10.1016/J.ENERGY.2014.10.080.

[41] Bekdemir C, Baert R, Willems F, Somers B. Towards Control-Oriented Modeling of Natural Gas-Diesel RCCI Combustion, 2015. doi:10.4271/2015-01-1745.

[42] Kothari A. Automatic Tuning Procedure for XCCI. TNO, 2017.

[43] Chang J, Güralp O, Filipi Z, Assanis DN, Kuo T-W, Najt P, et al. New Heat Transfer Correlation for an HCCI Engine Derived from Measurements of Instantaneous Surface Heat Flux, 2004. doi:10.4271/2004-01-2996.

[44] Goodwin DG, Harry K. Moffat, Raymond L. Speth. Cantera: An object- oriented software toolkit for chemical kinetics, thermodynamics, and transport processes 2018, Version 2.4.0. doi:10.5281/zenodo.170284.

[45] Peters N, Paczko G, Seiser R, Seshadri K. Temperature cross-over and non-thermal runaway at two-stage ignition of n-heptane. Combustion and Flame 2002;128:38–59. doi:10.1016/S0010-2180(01)00331-5.

[46] Smith G.P., Golden, D.M., Frenklach, M et al. GRI-MECH 3.0 2018, http://www.me.berkeley.edu/gri_mech/ (accessed February 03, 2018).

[47] Heywood JB. Internal combustion engine fundamentals 1988.

[48] Caterpillar Marine Diesel Engines and Generators: Value-based equipment selection guide n.d. http://s7d2.scene7.com/is/content/Caterpillar/C10317480 (accessed May 10, 2018).

[49] Rahnama P, Paykani A, Reitz RD. A numerical study of the effects of using hydrogen, reformer gas and nitrogen on combustion, emissions and load limits of a heavy duty natural gas/diesel RCCI engine. Applied Energy 2017;193:182–98. doi:10.1016/J.APENERGY.2017.02.023.

[50] Splitter D, Wissink M, Kokjohn S, Reitz RD. Effect of Compression Ratio and Piston Geometry on RCCI Load Limits and Efficiency, 2012. doi:10.4271/2012-01-0383.

[51] Selim MYE. Sensitivity of dual fuel engine combustion and knocking limits to gaseous fuel composition. Energy Conversion and Management 2004;45:411–25. doi:10.1016/S0196-8904(03)00150-X.

[52] Jia M, Gingrich E, Wang H, Li Y, Ghandhi JB, Reitz RD. Effect of combustion regime on in-cylinder heat transfer in internal combustion engines. International Journal of Engine Research 2016;17:331–46. doi:10.1177/1468087415575647.

[53] Jemni MA, Kantchev G, Abid MS. Influence of intake manifold design on in-cylinder flow and engine performances in a bus diesel engine converted to LPG gas fuelled, using CFD analyses and experimental investigations. Energy 2011;36:2701–15. doi:10.1016/J.ENERGY.2011.02.011.

[54] Hwang JT, Kane SP, Northrop WF. Demonstration of Single-Fuel Reactivity Controlled Compression Ignition Using Reformed Exhaust Gas Recirculation, 2018. doi:10.4271/2018-01-0262.

[55] Hunicz J, Mikulski M. Investigation of the thermal effects of fuel injection into retained residuals in HCCI engine. vol. 228C. 2018. doi:10.1016/j.apenergy.2018.07.075.

APPENDIX A – GOVERNING EQUATIONS OF THE XCCI MODEL

This appendix discusses the governing equations of the XCCI multi-zone model. The underlying assumptions for the specific sub-models are explained in section 2.2. Note that the equations were already presented, among others in [41]. This description adopts the same nomenclature for consistency and slightly extends the description to highlight the specific modifications introduced during the development process. The model is based on the first law of thermodynamics, which for a multi-zone approach can be written as follows:

$$m_z c_v \frac{dT_z}{dt} = -\sum_{i=1}^{N_s} e_i \frac{dm_{z,i}}{dt} - p\frac{dV_z}{dt} + \sum_{i=1}^{N_s} \dot{m}_{z,i}^{in} h_i(T_{in}) + \sum_{i=1}^{N_s} \dot{m}_{z,i}^{out} h_i(T_z) + \dot{Q}_z + \dot{Q}_{z,T}^{D} + \sum_{i=1}^{N_s} \dot{m}_{z-1,i}^{D} h_i(T_{z'}) + \sum_{i=1}^{N_s} \dot{m}_{z+1,i}^{D} h_i(T_{z''}), \qquad z \in [1, N_z] \tag{A1}$$

Here subscripts z and i denote the zone and species number respectively. The annotation c_v is the specific heat capacity at constant volume. N denotes the number of species and zones respectively. The variables m, p and T with the subscript z refer to the total mass, pressure, and temperature of the charge in the given zone, while $m_{z,i}$, e_i and h_i are the mass, internal energy, and enthalpy of the individual species (i) respectively. The third and fourth terms on the right-hand side define the enthalpy change caused by the mass flow ($\dot{m}_{z,i}^{in/out}$) through the cylinder boundaries. Here the flow through the engine valves and fuel injection process are explicitly considered with indexes in and out referring to ingoing and outgoing flow respectively. For the first process, flow rates are computed using standard formulas for the compressible fluid flow through a restriction, with consideration of choke [47]. The applied gas flow model accommodates the backflow phenomena and the accumulation of backflow in the intake runner. The fuel injection driven mass change is represented as a Gaussian profile normalized to the total fuel value within the designated injection timings. No spray penetration model is applied and the fuel is introduced to individual zones basing on a predefined fuel distribution factor - considered as a calibration parameter. The present study assumes a case dependent fuel distribution - basing on experimentally driven correlation on engine speed, injection timings and BR [42].

The term $\dot{Q}_z$ describes the heat transfer rate due to heat loss and evaporative cooling during fuel injection. This is already discussed in section 2.2. $\dot{Q}_{z,T}^{D}$ represents the heat transfer between the zones. This is modeled as:

$$\dot{Q}_{z,T}^{D} = A_{z,z-1} C_t \lambda \left(\frac{\Delta T}{\Delta R}\right)_{z,z-1} + A_{z+1,z} C_t \lambda \left(\frac{\Delta T}{\Delta R}\right)_{z+1,z}, \qquad z \in [1, N_z], \tag{A2}$$

where $A_{z,z'}$ is the zone boundary area between the neighboring zones z and z' and ΔR denotes the distance between the respective centerlines (see Figure 4).Here, λ is the laminar conduction coefficient and C_t is the turbulent diffusivity factor, constant in time and arbitrary the same for all zones. C_t is considered a calibration parameter for the model and is made case-dependent with a polynomial fit bounding it to engine speed, intake pressure, and diesel injection parameters [42].

Finally, the two terms closing Eq. A1, describe the enthalpy change due to inter-zonal mixing. This is assumed diffusion-based similarly to Eq. (A2):

$$\Delta \dot{m}_{z,i}^{D} = \dot{m}_{z-1,i}^{D} + \dot{m}_{z+1,i}^{D} = A_{z,z-1} C_t \frac{\lambda}{c_p Le_i} \left(\frac{\Delta Y_i}{\Delta R}\right)_{z,z-1} + A_{z+1,z} C_t \frac{\lambda}{c_p Le_i} \left(\frac{\Delta Y_i}{\Delta R}\right)_{z+1,z}, \qquad z \in [1, N_z] \quad \text{and} \quad i \in [1, N_s] \tag{A3}$$

where according to the Fick's Law, the c_p is the specific heat at constant pressure, while Le_i and Y_i are the Lewis number and the mass fractions of species i, respectively.

Note, that the total change in the mass of individual species takes in to account the chemical reactions, the fuel, intake and exhaust zonal flow, and the inter-zonal mixing:

$$\frac{dm_{z,i}}{dt} = \dot{\omega}_{z,i} V_z + \dot{m}_{z,i}^{in/out} + \Delta\dot{m}_{z,i}^{D}, \qquad z \in [1, N_z] \quad \text{and} \quad i \in [1, N_s], \tag{A4}$$

where the reaction kinetic driven net source term of species is defined as:

$$\dot{\omega}_i = M_i \sum_{i=1}^{N_r} (\nu''_{ij} - \nu'_{ij}) r_j, \qquad i \in [1, N_s], \tag{A5}$$

Here, M_i is the molar mass of individual species and N_r is the total number of reactions considered in the kinetic schema. If the reaction j is considered reversible, its net reaction rate can be written as:

$$r_j = k_j^f \prod_{i=1}^{N_s} \left(\frac{\rho Y_i}{M_i} \right)^{\nu'_{ij}} - k_j^r \prod_{i=1}^{N_s} \left(\frac{\rho Y_i}{M_i} \right)^{\nu''_{ij}}, \qquad j \in [1, N_r], \tag{A6}$$

with k_j is the reaction rate coefficient, ρ the density, and where subscripts f and r mark the forward and reverse reaction, respectively. The reaction rate coefficient is defined by the well-known Arrhenius expression:

$$k_j = \alpha_j T^{\beta_j} \exp\left(\frac{-E_a}{R_u T} \right), \qquad j \in [1, N_r],$$

where E_a refers to the activation energy and R_u to the universal gas constant. The parameters α and β are reaction rate constants.

Note that the coupling of the zonal temperature and composition to the in cylinder-pressure (assumed equalized across all zones) is governed by the equation of state. The zones may, therefore, expand or shrink (i.e. the volume of each zone changes) depending on the local conditions, but are constrained by the total in cylinder volume at the given crank angle. The instantaneous volume is calculated based on a standard relation to cylinder geometry, with consideration of the piston eccentricity [47].

APPENDIX B– XCCI MODEL FUNCTIONALITY CHECK ON LARGE-BORE GEOMETRY

This section discusses the scalability of the XCCI model from engine B to engine A (Table 2). From the portfolio of the tuned RCCI operating points (Fig. 6) a case similar to the available operating data of the considered large-bore engine is selected. The comparison of both operating points is provided in Table A1 (case 1 and 2). Case 2 in Table A1 corresponds to point 4 in Fig. 6.

Table A1: Parameters of LBDF and RCCI cases used to test XCCI model functionality on large-bore engine platform.

	Engine / mode	N	BMEP	EGR	λ	BR	SOI	T_{IVC}
		rpm	bar	%	-	%	CA	K
1	Engine A LBDF	720	20	-	Δ from base case			
2	Engine B RCCI	1002	9.8	-	base	-15	-14	+35
3	Engine A RCCI	720	18.5	-	base	-15	-14	+35

Disregarding the engine platform and loading, both operating points (case 1 and 2) have the same global mixture strength, yet efficient RCCI combustion is achieved at significantly lower BR and elevated T_{IVC} compared with LBDF. This is consistent with earlier research on NG-diesel RCCI pointing to the need to raise intake temperatures to boost combustion efficiency [30]. For the non-EGR case discussed here, it can be done by providing a bypass on the intercooler or reducing its efficiency. In addition, BR values of 80 – 90 % are indicated as most suitable for RCCI combustion (Table 1). Very early injection (Table A1 for the case 2) and the associated elongated diesel mixing period are characteristic of RCCI.

Since the XCCI model is solely suitable for simulating combustion regimes predominantly controlled by chemical kinetics, an initial attempt to realize case 1 failed to show hardly any combustion. Thus, based on the air-path and geometry prerequisites of case 1, (Table A1) case 3 is composed by adopting RCCI-favouring conditions of case 2 (BR, SOI, manifold temperature). The cumulative fuel energy input is scaled up to match load requirements of case 1.The results of running case 3 on the XCCI model with MAN geometry with respect to experimental data from the LBDF engine (case 1) are shown in Fig. A2. For comparison, the results of the case 2 simulation (geometry of engine B) with respect to TNO's heavy-duty RCCI engine measurements are shown in Fig. A1.

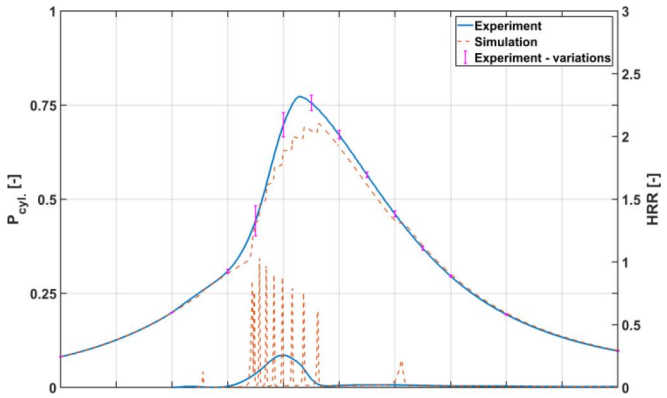

Fig. A1: Results (in-cylinder pressure and heat release) of simulating RCCI on the TNO platform (case 2) vs the corresponding reference experimental data. Error bars represent mean cycle-to-cycle variations. The values are scaled to the adopted P_{max} and peak HRR limits.

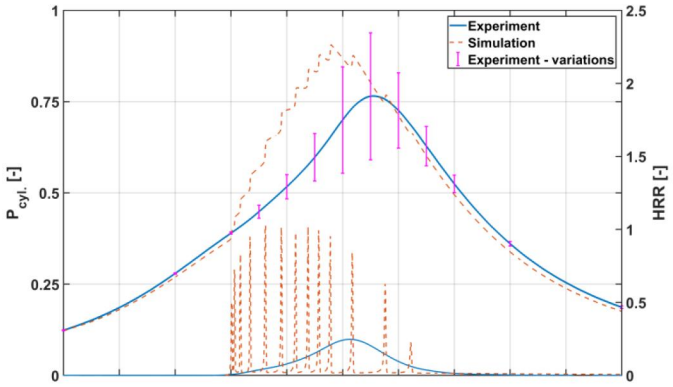

Fig. A2: Results (in-cylinder pressure and heat release) of simulating RCCI on the large-bore engine platform (case 3) vs the corresponding LBDF reference experimental data for this engine (case 1). Error bars represent mean cycle-to-cycle variations. The values are scaled to the adopted P_{max} and peak HRR limits.

Figure A1 shows that the XCCI model reproduces RCCI-case in-cylinder pressure with an accuracy level close to the cycle-to-cycle variations. The extent to which this translates to the ability to reproduce engine parameters and emissions is shown in Fig. 6, where case 4 corresponds to the results presented in Fig. A1. Note that crank angle at 50% heat released (CA50), P_{max} and IMEP are well within cylinder-to-cylinder variations.

Figure A2 shows that RCCI combustion (simulated - case 3) has fundamentally different characteristics than LBDF combustion (experimental - case 1). LBDF heat release rises slowly from the start of combustion at around -10 CA to reach a maximum at around 10 CA aTDC. RCCI heat release is notably faster and rises quickly after start of combustion. The "spiky" characteristic of the simulated heat release is due to the model's zonal nature. Also note the rather large levels of cycle-to-cycle variations in the LBDF combustion. This is reported to be common for micro-pilot pilot ignited, lean-burn gas engines [12, 13].

Case 2 in Fig. A1 simulates TNO's RCCI heavy-duty truck engine. It shows similar combustion characteristics to case 3, simulating a large-bore engine (Fig. A2). The major difference is that combustion is significantly faster for smaller engine, yet the large-bore engine shows higher peak heat release rate (HRR) values. The first observation is explainable by lower engine-speed and thus lower turbulence levels for the large-bore unit. Turbulence has proven to have an accelerating effect on RCCI HRR [30, 31]. The second phenomenon is simply caused by higher amount of energy/per cylinder-volume being released for case 3 (the IMEP is almost double of that of case 2). The higher load is also responsible for slightly earlier start of combustion with the large-bore engine.

This fundamental consistency in the simulation results between case 2 (TNO's heavy-duty truck engine geometry, for which the model was originally tuned) and case 3 (large-bore engine) support the conclusion that the XCCI model is scalable and thus valid for the scope of the present research. Furthermore, the above conclusion is reinforced by proper parameter sensitivity. The influence of individual parameters on large-bore RCCI combustion, from the efficiency and emissions point of view, is discussed in detail in Appendix D.

APPENDIX C – THE RESULTS OF CLUSTER SIMULATIONS FOR FULL LOAD AND NEAR-IDLE CONDITIONS

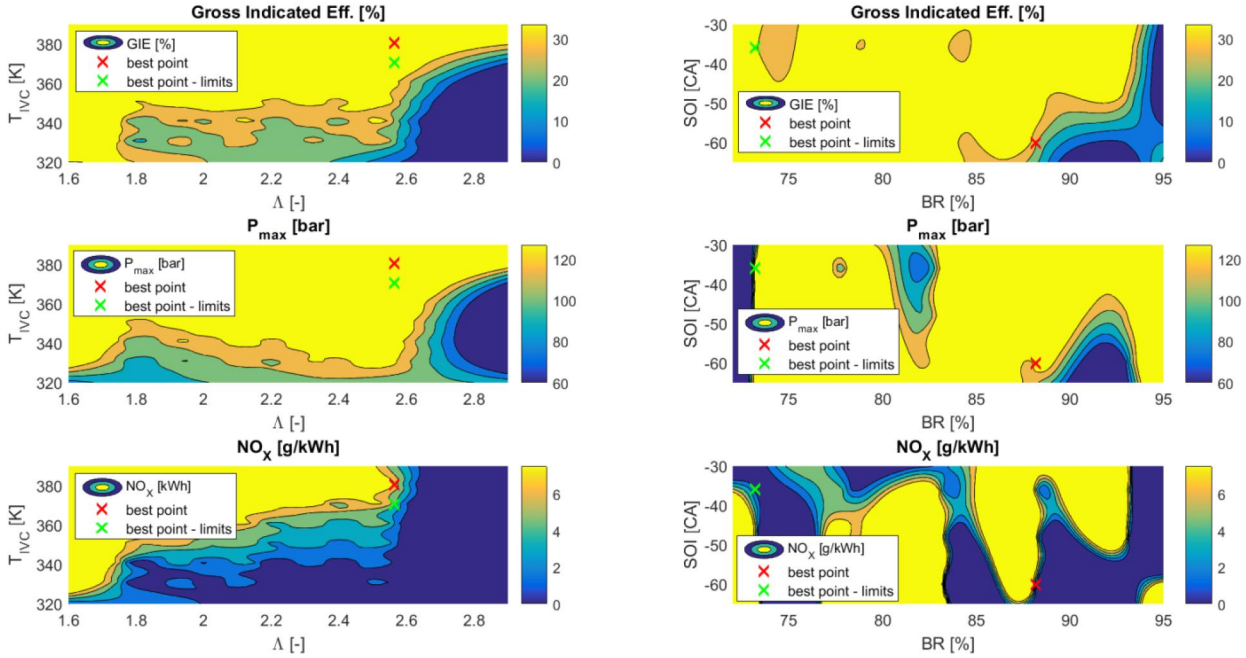

Fig. A3: Efficiency, peak pressure and NO_x emissions for the 100% load / no-EGR case mapped on the optimization parameters matrix. The left and right plots show the maps with respect to the air-path and fuel-path variables respectively.

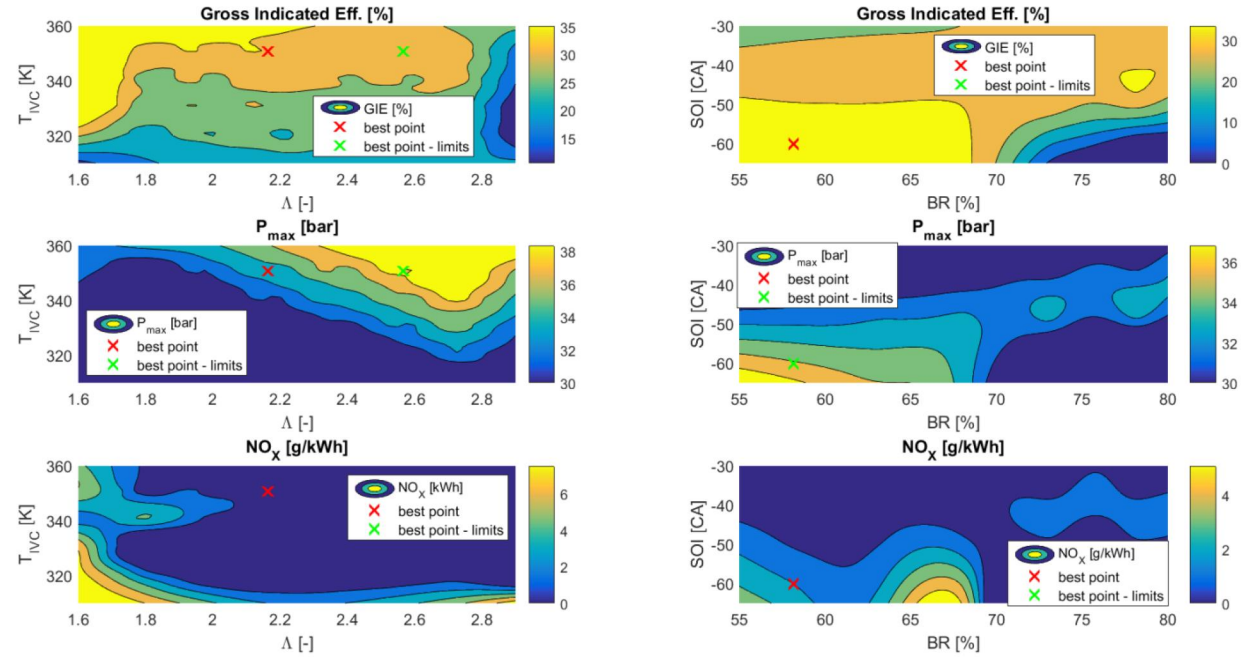

Fig. A4: Efficiency, peak pressure and NO_x emissions for the 25% load / no-EGR case mapped on the optimization parameters matrix. The left and right plots show the maps with respect to the air-path and fuel-path variables respectively.

APPENDIX D – RCCI OPERATIONAL PARAMETERS SENSITIVITY

This subsection aims to provide additional understanding on how individual operating parameters impact RCCI combustion efficiency and emissions. All results are based on the optimized 75% load, lean RCCI case (Table 5) and represent individual parameter sweeps around this baseline.

IVC temperature

Figure A5 presents the effect of changing the T_{IVC} on RCCI combustion (black circles). Red crosses mark the baseline, optimized point. T_{IVC} has a significant effect on combustion phasing, efficiency and emissions. With other engine parameters unchanged, lowering T_{IVC} by just 10 K from the optimized value reduces combustion efficiency by 8 percentage points. In this case, that reduction in combustion efficiency translates to THC emissions of over 8g/kWh, associated mainly to unburned CH_4. The consequent drop in indicated efficiency is additionally worsened by the CA50 moving away from TDC. The trend in CA10 (Fig. A5) shows how the start of combustion is affected strongly by T_{IVC}. Peak pressure reduces with lower T_{IVC} due to incomplete and retarded combustion.

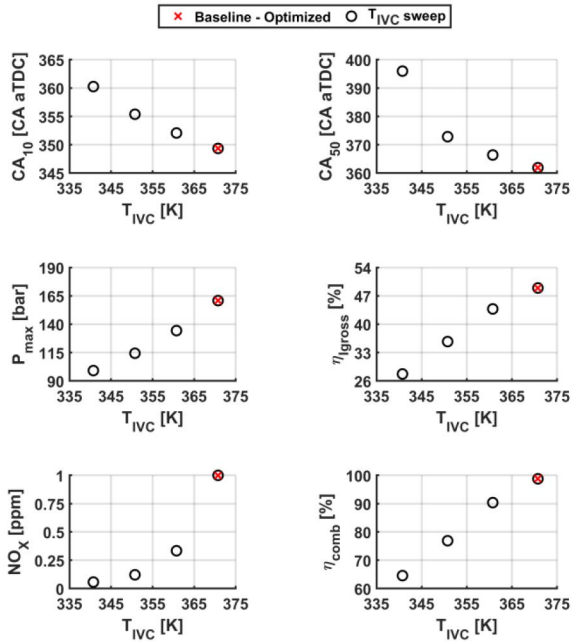

Fig. A5: Effect of T_{IVC} on a 75%-load case, RCCI combustion. NO_x emissions are scaled such that the baseline optimized point = 1.

The mixture could not ignite at all temperatures below 340 K so points below this value are not shown in Fig. A5. This figure also shows that the discussed 75%-load RCCI case had optimized at the highest explored T_{IVC} of 371 K. The GT-Power simulations confirmed that higher temperatures are attainable at this operating point, by further reducing intercooler efficiency (limit at 398 K). However, analyzing Fig. A5's trends in combustion efficiency and NO_x emissions suggests that further attempts to increase T_{IVC} would result in exceeding the Tier III emission limits without providing additional THC/CO reduction. NO_x emissions increase exponentially with intake temperature. This conclusion is also supported by the results from the 100%-load case. Here, the optimized point is reached at the same T_{IVC} value of 371 K, while the imposed exploration range in this parameter was set at 381 K.

Mixture strength

Figure A6 reveals the influence of mixture strength (λ) on RCCI combustion. One can observe that higher λ supports achievement of high indicated efficiencies. This results directly from higher ratios of specific heats for lean mixtures, which directly influences thermodynamic efficiency [47]. Note that while indicated efficiency is increasing, combustion efficiency is slightly decreasing. The change in combustion efficiency also changes the balance of the trade-off NO_x and THC/CO emissions. Figure A6 shows NO_x increasing dramatically towards stoichiometric mixture.

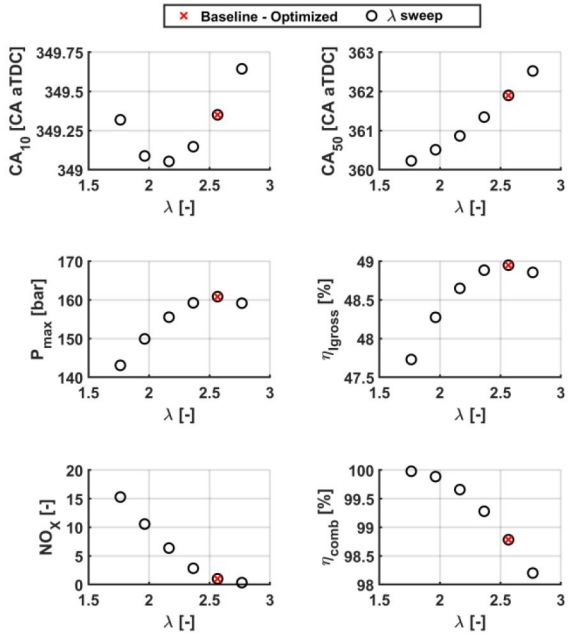

Fig. A6: Influence of mixture strength (λ) on RCCI combustion. NO_x emissions are scaled such that the baseline optimized point = 1.

Note that at a given operating point, λ has no major effect on start of combustion, yet the combustion duration is elongated to some extent. This is evident from the difference between CA10 and CA50 in Fig. A6. This inhibits attainment of higher indicated efficiencies and explains the drop in combustion efficiency: combustion tends to quench due to temperature decrease at expansion. The indicated efficiency trend line peaks with λ around 2.6: further leaning of the mixture means that losses from incomplete combustion and prolonged combustion start to overcome the benefits of higher specific heats.

Importantly, Fig. A6 shows that peak pressure generally increases with higher λ, which may pose additional limits while operating at higher loads. This is associated mainly with higher boost pressures and consequential higher IVC trapped masses.

Blend Rate

The Blend Rate definition used here is introduced Eq. 1. Lower values of this parameter indicate more diesel being injected with the same total fuel energy. Figure A7 shows the BR sweep around the optimized 75% load case with no EGR. Note that for the given condition, the sweep was performed for BR up to 95%, but the mixture failed to ignite at points beyond 88%. These points are omitted in Fig. A7 to avoid over-extending the y-axis.

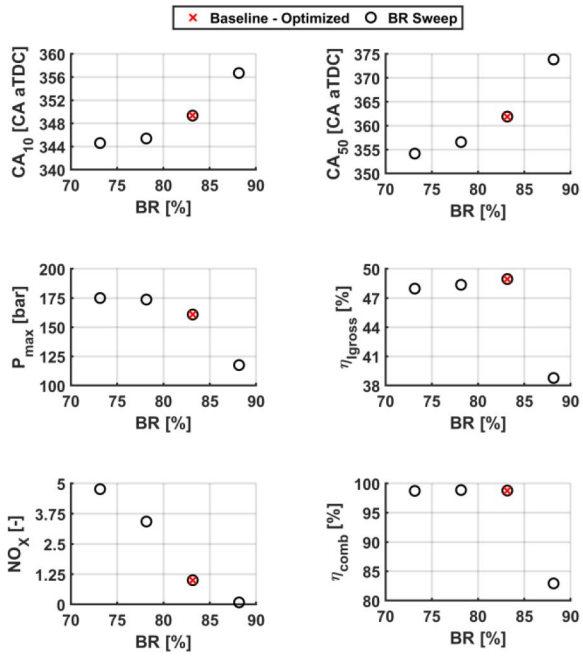

Fig. A7: BR sweep around the optimized 75% load case with no EGR. NO_x emissions are scaled such that the baseline optimized point = 1.

Figure A7 illustrates how BR affects the combustion phasing to a large extent. CA10 can be influenced by as much as 14 CA with relatively small increase in BR from 73% to 88%. Generally, lowering BR gives an earlier start of combustion. At the same time, NO_x emission increases significantly because larger amounts of diesel fuel injected directly into the cylinder introduce locally richer mixtures. The resultant reactivity stratification reduces ignition delay and causes local combustion temperatures to peak, further elevating NO_x emissions. Note that the CA10 retards with increased BR only to a certain extent and reaches saturation around 345 CA. At this point, the mixture becomes locally too rich and the oxygen entrainment rate starts to limit the start of combustion.

The combustion efficiency remains high for BR from 70% to 85%. It is actually slightly lower for lower BR due to unburned diesel particles and CO forming in areas with limited oxygen availability. Combustion efficiency collapses rapidly if the BR is above 85%, indicating existence of a rigorous misfire limit at the given IVC conditions. This is caused by late ignition and slow combustion, which quenches due to the temperature drop in the expansion phase. Note that the best efficiency, together with low emission footprint, is always acheved at the highest BR commensurate with correct combustion phasing and associated misfire limit.

In-cylinder turbulence

In the XCCI model the turbulence level is reflected in a form of turbulent mixing coefficient (Ct). This was tuned and correlated with engine load (boost pressure) for the base engine B in [42]. This correlation is directly transferred to this study's model of the large-bore engine. However, the large-bore engine can utilize turbulence to a different extent, so here we study how changing the Ct parameter affects the baseline, optimized RCCI point performance. Figure A8 presents the simulation results of changing the Ct on the performance of the large-bore engine. This is discussed in terms of combustion indicators (CA50, P_{max}), efficiency and emissions. The baseline point is indicated in light blue.

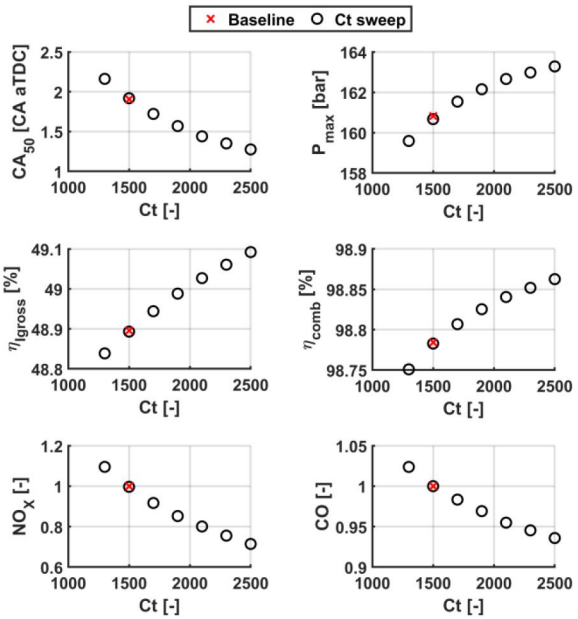

Fig. A8: Simulated effect of wide-range change in the turbulent mixing coefficient, on the performance of the research engine. NO_x and CO emissions are scaled such that baseline point = 1.

Figure A8 shows that the model anticipates the correct fundamental trends associated with turbulence influence. CA50 shifts towards TDC with increased Ct, indicating faster combustion. Indicated efficiency also rises with increased Ct. Fuel oxidation is also more complete, shown by the rising combustion efficiency plot. Note however, that the potential gain in combustion efficiency is relatively small. The gain is less than 0.1 percentage point, despite increasing the Ct from the baseline value of 1500 to 2500, which is considered the upper limit of attainable turbulence. This insensitivity stems mainly from the fact that the baseline is already optimized, in terms of operating conditions, for high combustion efficiency. Note that combustion efficiency reaches saturation at around 99%.

The absolute shift in CA50 produced by high Ct is also rather small: around 0.8 CA higher than at baseline Ct. This, together with the combustion efficiency improvement, translates to the possibility that increased turbulence would generate an overall gross indicated efficiency increase of around 0.2 percentage points at the given 75%-load point. It is worth mentioning that larger efficiency gains from better in-cylinder mixing can be expected for RCCI at low engine-loads. This regime typically encounters issues with combustion efficiency due to low baseline turbulence from low boost pressures [31] and insufficient manifold temperatures [40]. However, high turbulence does present a challenge for high-load RCCI operation because it increases peak pressure, as seen in Fig. A8.

Despite the above limitations, increasing in-cylinder turbulence is one of the few strategies immune to the THC/NO_x trade-off. Figure A8 shows how both NO_x and CO emissions decline as Ct increases. Both trends can be easily explained by increased fuel dilution in the pre-combustion (mixture preparation) phase. More extensive mixing produces locally leaner mixtures, leading to lower combustion temperatures and hence less NO_x. CO emissions are reduced mainly due to higher oxygen entrainment rates.

Declaration of interests

☒ The authors declare that they have no known competing financial interests or personal relationships that could have appeared to influence the work reported in this paper.

☐The authors declare the following financial interests/personal relationships which may be considered as potential competing interests:

On behalf of the authors, Maciej Mikulski.

1. Feasibility of RCCI for mid-speed gas engines is assessed for the first time
2. Simulations optimize efficiency within hardware and emissions constraints
3. CH4 slip is below 1 g/kWh with baseline efficiency using stock hardware
4. Hardware-optimized RCCI can deliver superior indicated efficiency of 52%
5. 52% efficiency attainable while meeting tough EU-Stage V emission limits